Journal of
Civil
Engineering
Researchers

Chief Editorial:
Morteza Jamshidi

Managing Editor:
Kamyar Bagherineghad

J-Researchers

Volume 5, Number 3, September 2023

Contents

**JOURNAL OF
CIVIL
ENGINEERING
RESEARCHERS**

Seismic Performance Evaluation of Friction Damper and Yielding Metallic Damper in Steel Frame

Mohammadreza Oliaei [a*], Mahdi Mashhadiyan [a], Reza Forootan [a]

aDepartment of Civil Engineering, Ramsar Branch, Islamic Azad University, Ramsar, Iran

Abstract

In recent decades, various control systems have been studied to reduce the vibrations of structures under dynamic forces. Generally, types of structural control systems are classified into energy dissipation systems and seismic isolation systems. Examples of energy dissipation systems include metallic yielding dampers, friction dampers, viscoelastic dampers, viscous dampers, tunable mass dampers, and tunable liquid dampers. This article investigates the seismic performance of friction dampers and metallic yielding dampers in steel frames, as well as the performance of a two-story steel frame strengthened with metallic yielding dampers and combined with friction dampers. For this purpose, five two-story steel frames with eight-story divergent braces were examined: a frame without a damper, a two-story frame with metallic yielding dampers, a two-story frame with friction dampers, a two-story frame with the first floor having friction dampers and the second floor having metallic yielding dampers, and a two-story frame with the first floor having metallic yielding dampers and the second floor having friction dampers. The results show that the use of dampers increases the energy dissipation of the structure and reduces the maximum displacements induced in the structure as well as the base shear. The effect of metallic yielding dampers on reducing the base shear is greater than that of friction dampers, while the effect of friction dampers on increasing energy dissipation and reducing displacements induced in the structure is greater compared to metallic yielding dampers. © 2017 Journals-Researchers. All rights reserved. (DOI:**https//doi.org/10.52547/JCER.5.3.1**)

Keywords: Yielding metallic damper; Friction damper; Energy dissipation; Displacement; Base shear

1. Introduction

An earthquake is an unpredictable event that can occur at different times and intensities, destroying structures. Therefore, retrofitting structures against this phenomenon is inevitable. Usually, moderate earthquakes do not significantly affect the integrity of existing structures, while strong earthquakes reveal their strengths and weaknesses. Earthquakes such as the Northridge earthquake in the United States (1994) and the Kobe earthquake in Japan (1995) have had a significant impact on changing seismic codes and design methods for earthquake-resistant structures [1].

_____

* Corresponding author. Tel.: +98-911-392-4331; e-mail: m.r.oliaei@gmail.com.

Conventional structures absorb seismic energy by yielding or fracturing building materials. For example, when beams and columns create plastic hinges, or when concrete structures develop cracks or non-ductile components reach the failure stage, energy absorption occurs. Dampers provide a solution for yielding or dissipating energy, which is a method of absorbing seismic energy. These devices can absorb the majority of earthquake energy and keep the structure intact and ready for immediate use after an event [2].

In recent decades, various control systems have been studied to reduce structural vibrations caused by dynamic forces. Generally, types of structural control systems are divided into two categories: energy dissipating and seismic isolation systems. Examples of energy-dissipating systems include metallic dampers (yielding), friction dampers, viscoelastic dampers, viscous dampers, tuned mass dampers, and liquid dampers [3].

In general, seismic control systems are classified into four types: passive, active, semi-active, and hybrid control systems [3]. Devices that do not require external energy to function are called passive control devices. These systems are more reliable because they continue to work even if the energy source, which is likely to be interrupted during an earthquake, is cut off. Since these devices are located inside the structure and do not have an external energy source, they never change the internal energy of the structure and are incapable of destabilizing the structure [4, 5]. However, most passive control devices, such as friction sliding, yielding of metal, and deformation in viscoelastic bodies or fluids, work after a certain stage and can be designed not to be active in low lateral forces [6]. Yielding dampers and friction dampers are among the passive control systems.

Multiple research studies have been conducted on the application of various types of dampers in different structures. Mirzaifi and colleagues [7] concluded in their research that friction dampers introduce a counter-directional force to the structural movement, opposing the motion of the building and dissipating a considerable amount of input energy. Khaleghiyan and Tehranizadeh [8] demonstrated in their studies that friction dampers have a special capability in reducing the seismic energy of a structure. Bayat et al. [9] showed that the use of friction dampers increases the ductility of a structure. Karami and Sarmast [10], as well as Papadopoulos et al. [11], demonstrated that friction devices significantly improve the seismic resistance and damage control potential of braced and skeletal structures. Amiri [12] demonstrated in their research that properly distributed friction dampers can effectively control lateral displacement and diaphragm rotation. Latorre et al. [13], Manatori et al. [14], and Moneer et al. [15] concluded in their analyses that adding friction dampers to moment frames reduces the displacement by approximately 15%.

Kamasi et al. [16] investigated the effect of using steel-yielding dampers on the behaviour of structures and found that shape-adaptive structures equipped with steel-yielding dampers exhibit greater ductility and less displacement. Vada et al. [17] showed that steel-yielding dampers exhibit stable hysteretic behaviour and gradually increase the stiffness of the structure, improving its capacity to absorb energy. Li et al. [18] and Chan et al. [19] demonstrated that the use of steel-yielding dampers significantly increases the ultimate energy absorption capacity of the structure. Oh et al. [20] showed that increasing the length of the damper enhances the connection strength in skeletal structures. Their investigations also revealed that energy dissipation and plastic deformation are concentrated in the yielding dampers, preventing the non-elastic behaviour of beams and columns. Khoshnoodian and Kiani [21] found that adding a certain number of dampers to each floor effectively improves the structural response, but exceeding that number has no significant effect on the structural response improvement. Tohidi Moghadam and Saeed Monir [22] investigated a new type of circular-shaped yielding dampers and demonstrated that using these dampers in a concentrically braced frame system yields better performance compared to the beam-to-column connection, resulting in a noticeable reduction in displacement and base shear. Safari et al. [23] proposed new samples of yielding dampers for improving the ductility of moment connections and conducted an extensive investigation on them.

In this project, the seismic performance of friction dampers, yielding metal dampers, and their combination in a steel frame, as well as the performance of a two-story steel frame with yielding metal dampers, friction dampers, and their

combination, will be analyzed. The ultimate goal of the project is to examine the effects of using yielding metal dampers, friction dampers, and their combination in a two-story steel frame on the maximum lateral displacement, base shear, and energy dissipation of the structure.

2. Friction Dampers

Friction is used as an agent for energy dissipation. Mechanical engineers have long utilized this mechanism to dissipate the kinetic energy of moving bodies. Friction brakes are an example of friction application in the industry. The application of friction in structural engineering has led to the development of friction dampers, which absorb a significant amount of input energy from earthquakes and other dynamic excitations [24]. These types of dampers work based on the friction mechanism between solid bodies. Friction is an excellent energy dissipation mechanism and has been widely and successfully employed for dissipating kinetic energy. Various materials have been used for sliding surfaces. Examples include brake layers on steel, steel on steel, steel on bronze, and bolted connections with graphite combined with stainless steel and other metallic alloys. The choice of base metal for friction dampers is crucial. Corrosion can often reduce the assumed coefficient of friction for the desired service life. In reality, stainless steel alloys corrode and passivate, and their interfacial properties change over time, while bronze and brass increase the rate of corrosion when in contact with low-carbon alloys. In comparison, stainless steel does not show additional concerning corrosion when in contact with bronze, making it suitable for use in friction dampers. Friction dampers have very good performance characteristics. Their response is independent of frequency range and the number of independent loading cycles, thus offering a high potential benefit-to-cost ratio. These dampers fall into the category of hysteretic dampers. They dissipate energy through displacement and self-sliding [5]. All existing friction dampers essentially operate in the same way. One part remains stationary, while the other part dynamically slides on it. Slipping occurs at a certain level of force and moves according to Coulomb's friction law. No motion occurs until a specific force threshold is reached. However, after that, the sliding surface and motion begin. The combination and arrangement of these sliding surfaces create different types of friction dampers, including more complex configurations such as the Pall friction damper [24].

3. Yielding Metal Dampers

By understanding the crystal structure of various metals, we can examine the behaviour of metal yielding under cyclic loading conditions and observe desirable damping properties within the range before the yield point. By shaping a piece of metal into a form that exhibits yielding behaviour under dynamic structural loading (often in the form of an isosceles triangle) and placing it at the connection points between structural members, we can effectively utilize this property for energy dissipation and scattering during earthquakes. The material selection, shape, and placement of these types of dampers should be such that their damping properties are not significantly affected by various influencing factors over the lifetime of the structure. The metal used for constructing such dampers usually needs to exhibit suitable hysteresis behaviour, high fatigue endurance, relative strength, and minimal sensitivity to temperature changes. Essentially, metal dampers rely on the elastic deformation of the metal and the damping resulting from internal friction within the crystals. Various energy absorption systems can be used for this purpose. Yielding dampers are metallic devices that can dissipate energy in an earthquake through non-elastic deformations of the metals. These dampers typically yield in flexural, torsional, axial, or shear modes. They fall into the category of passive dampers in structures and contribute to increased damping and stiffness [2].

4. Analytical Modeling Compatibility Investigation Using Abaqus Finite Element Software

The modelling and validation of a yielding metal damper in Abaqus software were conducted for a laboratory specimen created by Lee et al. (2002) [18]. Abaqus is a unitless finite element software that does

not have default or changeable units. The units of different quantities are determined based on the input values of the program [26].

The element used for modelling the investigated shape memory yielding damper in this section is of the Solid type. The dimensions of different parts and the loading conditions are considered according to Figures 1 and 2. The geometric specifications of the model are given in Table 1, and the material properties of the steel used are provided in Table 2.
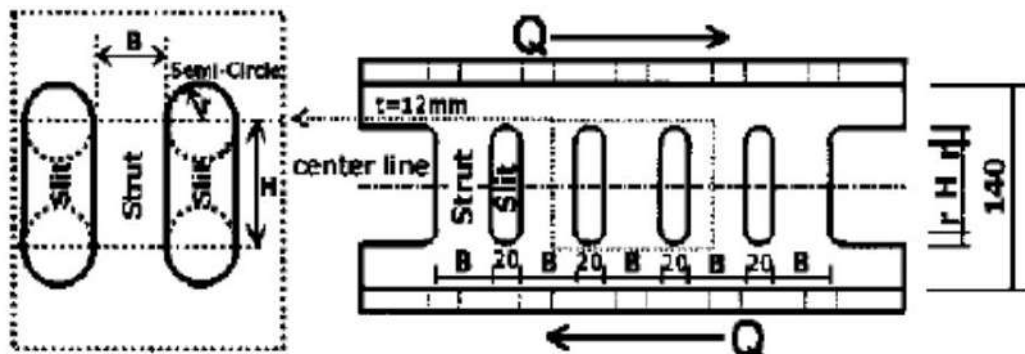

Figure 1: Investigated shape memory yielding metal damper specimen [18]

Table 1:
Geometric specifications of the investigated shape memory-yielding metal damper [18]

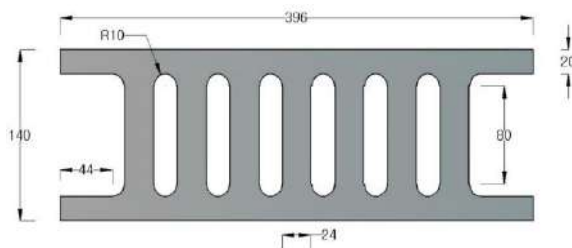| H (mm)	B (mm)	t (mm)	n	Case number
80	24	12	7	D0300-2

Figure 2: Geometric dimensions of the investigated shape memory-yielding metal damper specimen [18]

Table 2:
Material properties of the steel used in the investigated shape memory-yielding metal damper [18]

Elong (%)	σ_u (MPa)	σ_y (MPa)	υ	ρ (Kg/m3)	E (GPa)
28	451	307	0.3	7850	214

The shape of the elements used is HEX, as shown in Figure 3. For the used Solid element, an 8-node C3D8 mesh type is considered. It should be noted that the mesh size is 10x10 millimetres, resulting in 1380 elements.
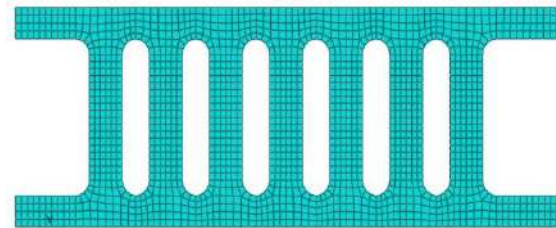

Figure 3: Partitioning and meshing of the investigated model

The bottom surface of the specimen is fully restrained in all directions.

$U_1=0$, $U_2=0$, $U_3=0$, $U_{R1}=0$, $U_{R2}=0$, $U_{R3}=0$

The specimen is subjected to only horizontal displacement in the X direction at the reference point with a linear magnitude of 66 millimetres, neglecting the effect of the specimen's weight. Contour plots of the von Mises stress distribution in the investigated specimen after loading and analysis are shown in Figure 4. The force-displacement curve of the numerical model created in Abaqus software and the experimental specimen are compared in Figure 5. The results indicate satisfactory agreement between the numerical and experimental models.
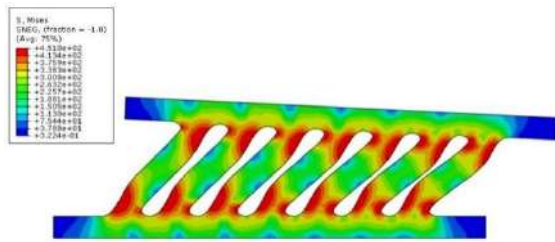
Figure 4: Contour plot of the von Mises stress distribution in the investigated specimen
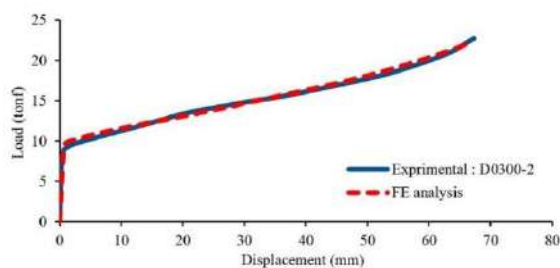

Figure 5: Comparison of the force-displacement curves of the experimental and analytical models

5. Modelling of structures in ETABS software

A two-story building with an eccentrically braced frame system has been designed. In this design, seismic considerations of the building design regulations against earthquakes (Standard 2800) have been taken into account. The design of the mentioned structure was performed using ETABS software. Then, based on the steel sections of beams, columns, and braces, the desired structural frames were simulated to investigate the forces generated in the members and the displacements of the nodes using ABAQUS software. Subsequently, considering the applied loads and their application to the structure, as well as based on the analysis cases, the system response and the desired parameters were determined.

The mentioned steel structures have a uniform plan on all floors, and each floor has an area of 200 square meters. The height of all floors is considered to be 2/3 meters. The lateral load-bearing system of the structure is moment-resisting frames in two orthogonal directions. The connection between beams and columns is simple. All components of the structure

are made of St37 steel with ultimate stress of 3700 kg/cm² and yield stress of 2400 kg/cm². The values of live and dead loads for the floors are 200 and 335 kg/m², respectively, and for the roof, they are 150 and 310 kg/m², respectively. The earthquake loads are obtained based on the assumption that the structure is located in seismic zone 4 of Iran. The roofs of the buildings are of block-and-beam type construction, and one-way slab reinforcement is considered. The structural plan and the three-dimensional image of the two-story frame modelled in the ETABS software are shown in Figures 6 and 7, and the results of the structural design are presented in Table 4.

After designing the structure in the ETABS software, a two-span structure with an eccentrically braced frame is selected, and the desired investigations are carried out by modelling it in the Abaqus software. In this study, 5 models with different arrangements have been used, and their specifications are given in Table 5.
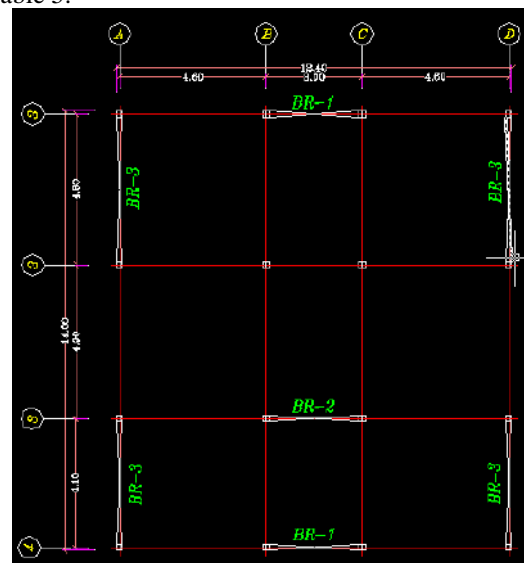

Figure 6: Structural plan under investigation

6. Modelling steps

To create the geometric shape of the members that will be later used for analysis, the Part module is used. Figure 8 shows the image of the modelled frame in the ABAQUS software.
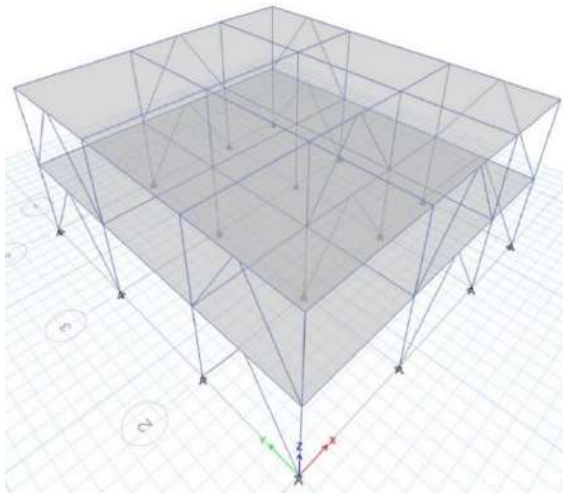
Figure 7: Three-dimensional image of a two-story steel structure with an eccentrically braced frame

Table 3:

Results of the design of the two-story steel structure

Story	Column	Beam	Brace
1	IPB240	IPE240	IPE140
2	IPB240	IPE240	IPE140

Table 4:

Arrangement of braces in the created models

Case No	Number of Stories	Type of Brace	Type of Damper in 1Story	Type of Damper in 1Story	The location of the Brace	Span length of the Damper
SP1	2	EB*	Without Damper	Without Damper	Outside Frames	Without Damper
SP2	2	EB	Metallic yielding Damper	Metallic yielding Damper	Outside Frames	4.8 m
SP3	2	EB	Friction Damper	Friction Damper	Outside Frames	4.8 m
SP4	2	EB	Metallic yielding Damper	Friction Damper	Outside Frames	4.8 m
SP5	2	EB	Friction Damper	metallic yielding damper	Outside Frames	4.8 m

* Eccentrically Brace

The type of analysis considered in this modelling is Dynamic-Explicit analysis. Moreover, Nlgeom is activated in the intended modelling, which means that Abaqus calculates nonlinear geometry. Considering nonlinear geometry in cases where loading on the model results in large displacements is very important [26].

In the software, the weld can be defined as either flexible or rigid, and the interaction between surfaces can be applied based on it. In this study, both pieces

are welded to each other using the tie constraint. Since the load must be applied to the centre of the part's surface during loading to avoid creating extra anchors, by defining a reference point at the floor level and constraining this point with multiple MPC constraints, the conditions can be applied.
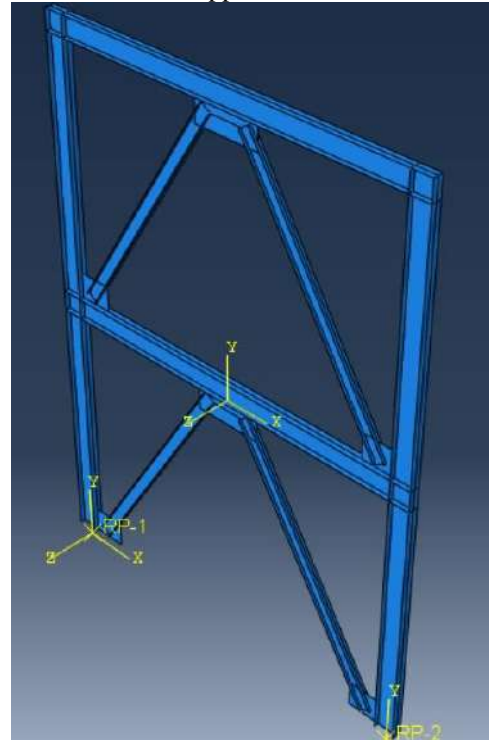

Figure 8: Image of a two-span two-story frame with an eccentrically braced frame modelled in the Abaqus software
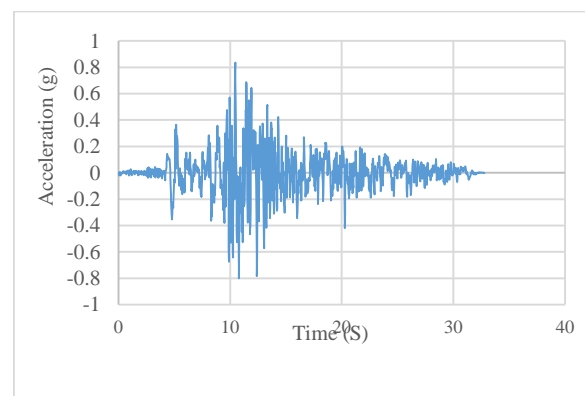

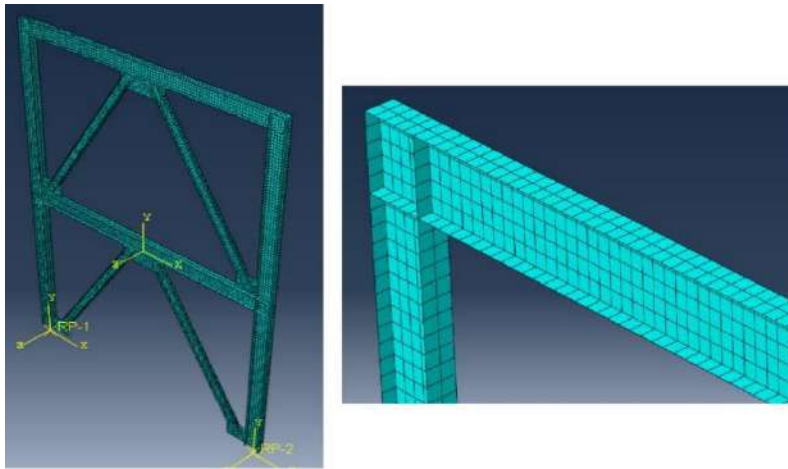Figure 9: Acceleration mapping of the Tabas earthquake in the X direction

Figure 10: Meshed frame with an eccentrically braced frame

The load applied to the structure is Tabas earthquake. The Tabas earthquake occurs in three directions: X, Y, and Z. The earthquake lasts 33 seconds, but since each earthquake consists of three parts: the initiation, effective, and fading phases, and the greatest impact and damage occur in the time interval of 4 to 20 seconds, therefore, considering that from the 20th second onwards, the acceleration has a negligible value, this time interval is used in the analyses, which reduces the computational time and leads to convergence of the results. Figure 9 shows the acceleration mapping of the Tabas earthquake in the X direction.

Considering the type of analysis and the mentioned explanations, reduced integration with three-dimensional stress family elements (C3D8R) and continuous node type technique have been used for meshing (Figure 10).

7. Investigation of the Targeted Frames

As mentioned, five frames (without a brace and with a yielding brace) are examined in this study. The hysteresis curves of each frame are analyzed to evaluate the load-bearing capacity, maximum displacements, and energy absorption and dissipation capabilities of the frames. Figures 11 and 12 depict the contour plots of Von Mises stress and Tresca stress in Frame SP1.
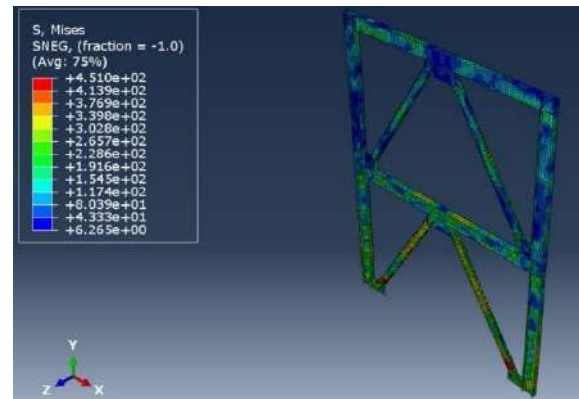

Figure 11: Contour plot of Von Mises stress distribution in the modelled frame in Abaqus software.
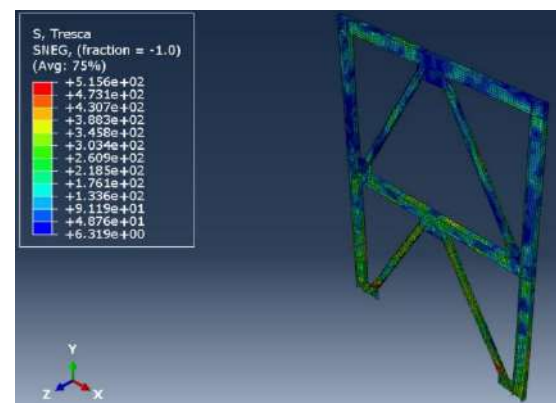
Figure 12: Contour plot of Tresca stress distribution in the modelled frame in Abaqus software.
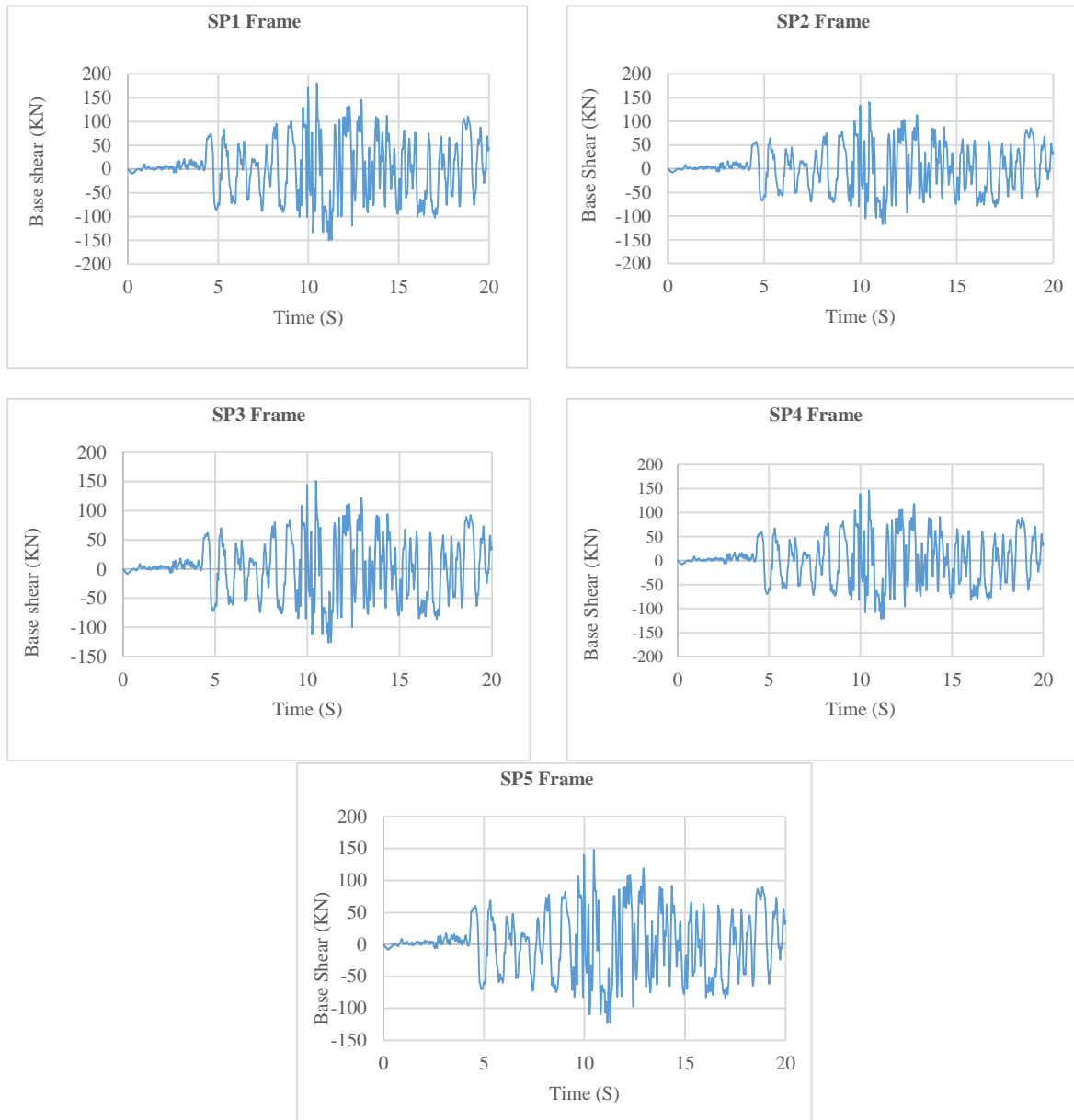
Figure 13: Base shear created in Frames SP1 to SP5

7.1. Investigation of Base Shear in the Examined Frames

The base shear in the braced frames with yielding and friction-based braces is evaluated based on the details provided in Table 5. The results are illustrated in Figure 13 and Table 5.

The examination of the obtained results indicates that the use of yielding braces and friction-based braces reduce the base shear in the investigated frames.
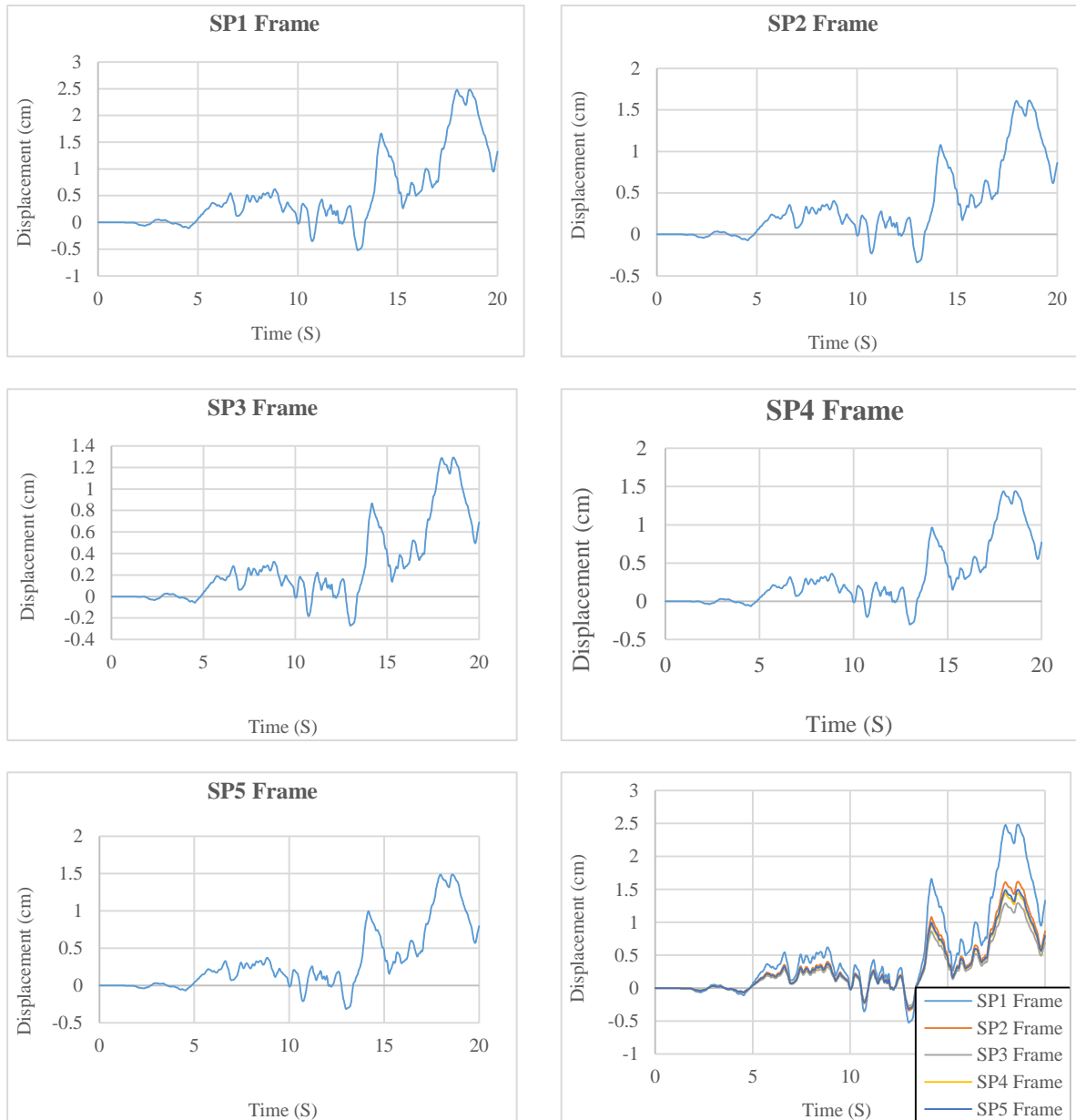
Figure 15: Maximum displacements created in Frames SP1 to SP5

The base shear in the frame where yielding braces are used in both stories is lower compared to the frame with friction-based braces in both stories. Therefore, it can be concluded that the influence of yielding braces on reducing the base shear is greater than friction-based braces. In Frames SP4 and SP5, where a yielding brace is used in one story and a friction-based brace is used in another story, no significant difference is observed in the base shear. The base shear in Frame SP4, which has a yielding brace in the first story and a friction-based brace in the second story, is slightly lower than Frame SP5.

Table 5:

Base shear imposed on the examined braced frames

Case Number	Base Shear (KN)
SP1	180.41
SP2	140.72
SP3	151.54
SP4	146.13
SP5	147.93

7.2. Examination of Maximum Displacements in the Examined Frames

The maximum displacements generated in the braced frames with yielding and friction-based braces are evaluated based on the details provided in Table 5. The results are presented in Figure 15 and Table 6.

Figure 15: Maximum displacements created in Frames SP1 to SP5

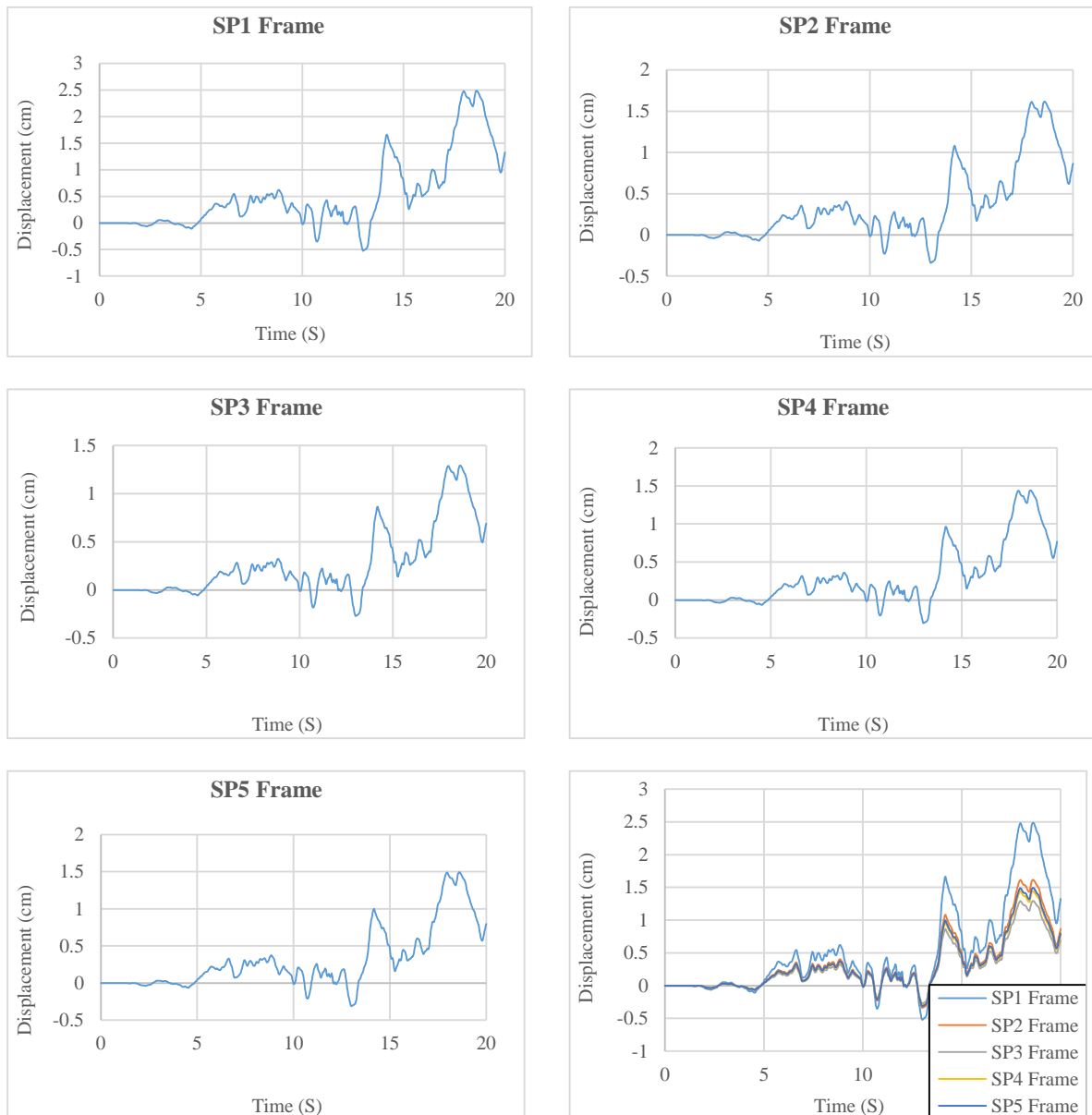The examination of the obtained results shows that the use of yielding braces and friction-based braces reduce the maximum displacements created in the examined frames. The maximum displacement in the frame where friction-based braces are used in both stories is lower compared to the frame with yielding braces in both stories. Therefore, it can be concluded that the influence of friction-based braces on reducing the maximum displacements created in the structure is greater than yielding braces. In Frames SP4 and SP5, where a yielding brace is used in one story and a friction-based brace is used in another story, no significant difference is observed in the maximum displacements. The maximum displacements in Frame SP4, which has a yielding brace in the first story and a friction-based brace in the second story, are slightly lower than Frame SP5."
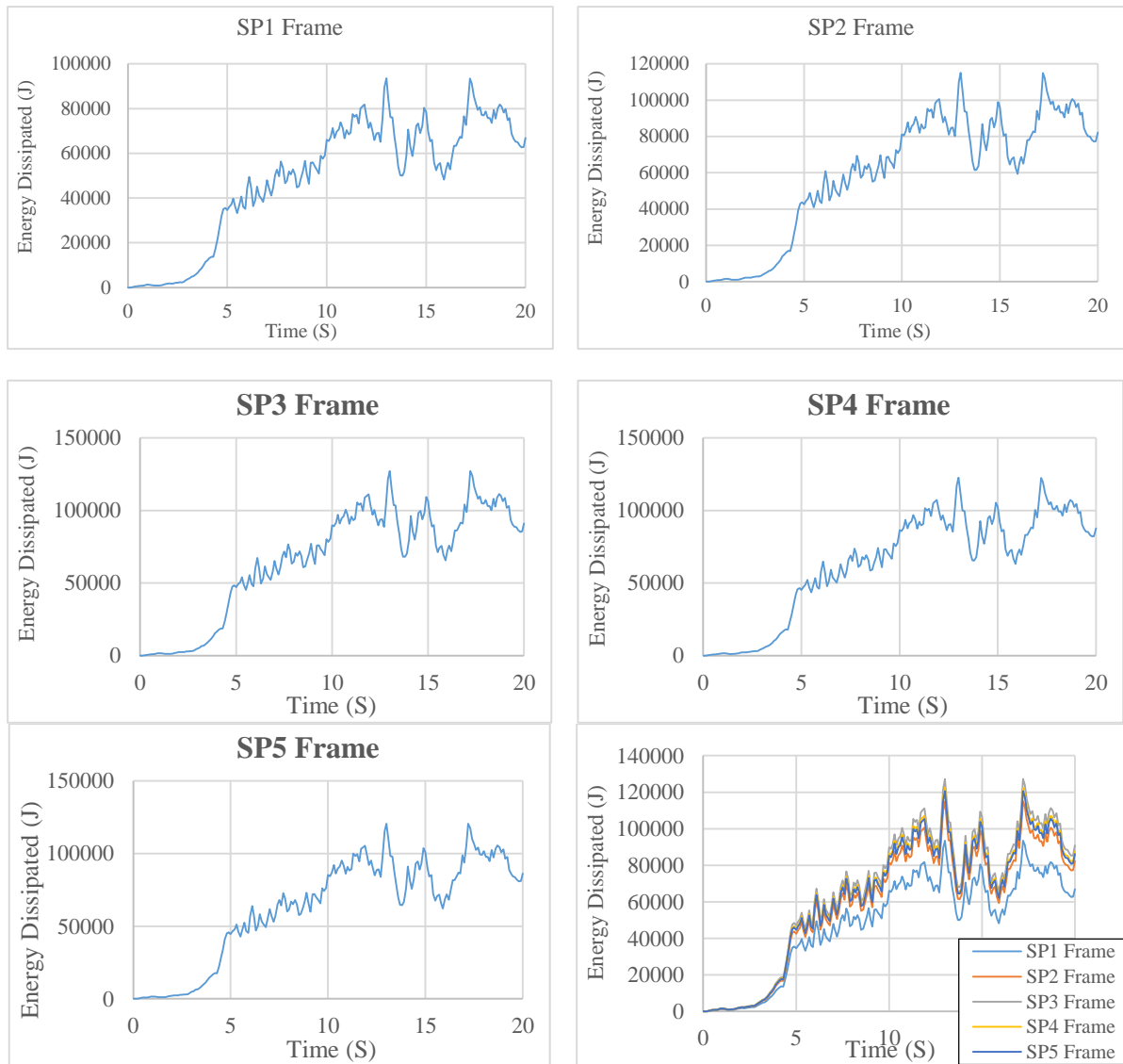

Figure 16: The energy absorption and dissipation capability in Case Numbers

Table 6:
Maximum displacements generated in the examined braced frames

Case Number	Maximum displacement(cm)
SP1	2.48
SP2	1.61
SP3	1.29
SP4	1.44
SP5	1.49

Table 7:

Maximum displacements generated in the studied braced frames.

Case Number	Maximum energy dissipated (J)
SP1	93509.6
SP2	115016.8
SP3	127173.1
SP4	122497.6
SP5	120627.4

7.3. Analysis of Energy Absorption and Dissipation Capability in the Studied Frames

The energy absorption and dissipation capability in frames braced with a divergent brace, in cases without the use of friction damper, and cases using friction and yielding metallic dampers are investigated, as detailed in Table 5, and the results are shown in Figure 16 and Table 7.

The analysis of the obtained results indicates that the use of yielding metallic dampers and friction dampers increases the amount of energy dissipated in the studied frame. The energy dissipated in a frame with friction dampers used in both stories is higher compared to a frame with yielding metallic dampers used in both stories. Therefore, it can be concluded that the influence of friction dampers on increasing the energy dissipated in the structure is higher than yielding metallic dampers.

In SP4 and SP5 frames where a yielding metallic damper is used in one story and a friction damper is used in another story, no significant difference in the dissipated energy in the structure is observed. The dissipated energy in the SP4 frame, where the first story has a yielding metallic damper and the second story has a friction damper, is slightly higher than in the SP5 frame. By examining the load-carrying capacity, maximum displacement generated, and energy dissipated in SP4 and SP5 frames, it seems that

using yielding metallic dampers in lower stories and friction dampers in upper stories has a greater impact on improving the behaviour of the structure. However, since the studied structure is a two-story frame, reaching a definitive conclusion requires examining multiple structures of low, medium, and high-rise buildings.

8. Conclusion

In this project, the seismic performance of a two-story steel frame with yielding metallic dampers, friction dampers, and a combination of yielding metallic dampers and friction dampers has been investigated. The results of the analysis are as follows:

- The use of yielding metallic dampers and friction dampers reduces the base shear in the frame.
- The base shear in a frame with yielding metallic dampers used in both stories is lower compared to a frame with friction dampers used in both stories. Therefore, it can be concluded that the influence of yielding metallic dampers on reducing the base shear is greater than friction dampers.
- In frames where a yielding metallic damper is used in one story and a friction damper is used in another story, no significant difference in the base shear of the structure is observed. The base shear in the SP4 frame, where the first story has a yielding metallic damper and the second story has a friction damper, is slightly lower than the SP5 frame.
- The use of yielding metallic dampers and friction dampers reduces the maximum displacements generated in the frame.
- The maximum displacement in a frame with friction dampers used in both stories is lower compared to a frame with yielding metallic dampers used in both stories. Therefore, it can be concluded that the influence of friction dampers on reducing the maximum displacements in the structure is greater than yielding metallic dampers.
- In frames where a yielding metallic damper is used in one story and a friction damper is used in another story, no significant

difference in the maximum displacements generated in the structure is observed. The maximum displacements in the SP4 frame, where the first story has a yielding metallic damper and the second story has a friction damper, are slightly lower than the SP5 frame.

- The use of yielding metallic dampers and friction dampers increases the amount of energy dissipated in the frame.

- The energy dissipated in a frame with friction dampers used in both stories is higher compared to a frame with yielding metallic dampers used in both stories. Therefore, it can be concluded that the influence of friction dampers on increasing the energy dissipated in the structure is greater than yielding metallic dampers.

- In frames where a yielding metallic damper is used in one story and a friction damper is used in another story, no significant difference in the energy dissipated in the structure is observed. The energy dissipated in the SP4 frame, where the first story has a yielding metallic damper and the second story has a friction damper, is slightly higher than the SP5 frame.

- By examining the load-carrying capacity, maximum displacements generated, and energy dissipated in the SP4 and SP5 frames, it seems that using yielding metallic dampers in lower stories and friction dampers in upper stories has a greater impact on improving the behaviour of the structure. However, since the studied structure is a two-story frame, reaching a definitive conclusion requires examining multiple structures of low, medium, and high-rise buildings. Thus, the findings suggest that the combination of yielding metallic dampers and friction dampers can effectively improve the seismic performance of steel frames. Further research on structures of different heights is recommended to validate these conclusions

References

[1] Mahin, S. A. (1998). Lessons from damage to steel buildings during the Northridge earthquake. Engineering structures, 20(4-6), 261-270.

[2] Shokouri, A. (2019). The role of the metal damper in improving the seismic performance of steel frames with rigid and semi-rigid connections. Master's thesis, Islamic Azad University, Ramsar Branch, Iran.

[3] Hassanzadeh, J. (2015). Performance evaluation of a yieldable metal damper. Master's thesis, University of Birjand, Birjand, Iran.

[4] Wilson, C. M. D. (2005). Fuzzy control of magnetorheological dampers for vibration reduction of seismically excited structures. The Florida State University.

[5] DiSarno, L., & Elnashai, A. S. (2002). Seismic retrofitting of steel and composite building structures. Mid-America Earthquake Center CD Release 02-01.

[6] Moradi, A. (2017). Performance investigation of multi-damper controlled structures with varying numbers of stories. Master's thesis, Islamic Azad University, Torbat Heydariyeh Branch, Iran.

[7] Mirsafi, H., Azhdari Moghadam, M., Ghalenooy, M., Kashtgar, B. (2011). Analysis of 4 and 8-story steel structures equipped with friction dampers using ABAQUS software. Sixth National Civil Engineering Congress, Semnan University, Iran.

[8] Khaleghian, F., Tehrani Zadeh, M. (2008). Design of a new type of friction damper with a brake pad. Journal of Seismology and Earthquake Engineering, 9(4).

[9] Bayat, M., Zahraei, M. (2016). The role of friction damper in improving the seismic performance of steel frames with rigid and semi-rigid connections. Journal of Structure and Steel, 19, Summer 2016.

[10] Karami Mohammadi, R., Sarmast, H. (2005). Use of braced frames with friction dampers for lightweighting in structures, First International Conference on Earthquake and Lightweight Construction.

[11] Papadopoulos, P. K., Salonikios, T. N., Dimitrakis, S. A., & Papadopoulos, A. P. (2013). Experimental investigation of a new steel friction device with link element for seismic strengthening of structures. Struct. Eng. Mech, 46, 4.

[12] Amiri, J., Rahimi, H. (2012). "Investigation of optimal slip percentage for friction damper in rehabilitated steel buildings with energy-based design concept", Third National Conference on Structure and Steel and First National Conference on Light Steel Structures (LSF).

[13] Latour, M., Piluso, V., & Rizzano, G. (2014). Experimental analysis on friction materials for supplemental damping devices. Construction and Building Materials, 65, 159-176.

[14] Montuori, R., Nastri, E., & Piluso, V. (2014). Theory of plastic mechanism control for the seismic design of braced frames equipped with friction dampers. Mechanics Research Communications, 58, 112-123.

[15] Saeed Monir, H., & Fazalipoor, N. (2016). Application of a new cylindrical slit damper for mitigation of structural

vibrations. Journal of Civil and Environmental Engineering, 45(81), 29-43.

[16] Kamasi, M., Sharifi, M. (2015). "Investigation and comparison of seismic behaviour of dissipative braced frames equipped with XADAS and TADAS dampers in terms of energy absorption, ductility, and displacement", Innovative Researches in Civil Engineering, Architecture, and Urban Planning, Tehran, International Sound and Vision Conferences Center.

[17] Wada, A., Huang, Y.H., Yamada, T., Ono, Y., Sugiyama, S., Baba, M., Miyabara, T. (1997). Actual size and real-time speed tests for hysteretic steel damper. Proceedings of Stessa, Vol. 97, pp. 778-785

[18] Lee, M. H., Oh, S. H., Huh, C., Oh, Y. S., Yoon, M. H., Moon, T. S. (2002). Ultimate energy absorption capacity of steel plate slit dampers subjected to shear force. Steel Structures, Vol. 2, pp. 71-79.

[19] Chan, R., Albermani, F. (2008). Experimental study of steel slit damper for passive energy dissipation. Engineering Structures, Vol. 30, pp. 1058-1066, 2008.

[20] Oh, S.H., Kim, Y.J., Ryu, H.S. (2009). Seismic performance of steel structures with slit dampers", Engineering Structures, Vol. 31, pp. 1997-2008.

[21] Khoshnoudian, F., Kiani, M. (2010). "Performance evaluation of Slotted Steel Damper (SSD) in steel structures with moment frame system", First National Conference on Earthquake-Geotechnics, Mazandaran, Babolsar.

[22] Moshtagh, A., Tohidi Moghadam, V. and Saeed Monir, H. (2012). Study of progressive fracture on reinforced frames with duct slit damper. The 2nd National Conference on Earthquake-Geotechnic and Structures, Mazandaran.

[23] Saffari, H., Hedayat, A.A., "Poorsadeghi Nejad, M. (2013). Post-Northridge connections with slit dampers to enhance strength and ductility", Journal of Constructional Steel Research, Vol. 80, pp. 138-152.

[24] Fathi, S. (2016). Optimal distribution of rotational friction damper properties in building floors. Master's thesis, Mohaghegh Ardabili University, Ardabil, Iran.

[25] Vader, A. S. (2004). The influence of signature tower passive energy dissipating devices on the seismic response of long-span cable-supported bridges (Doctoral dissertation, Washington State University).

[26] Abaqus User's Manual

Evaluation of integrated waste management by using of Waste Reduction Model (WARM)- (Case study of Amol-Noor region, Iran)

Seyed Mohammad Hosseini [ID][a*], Naser Mehrdadi [ID][b], Seyed Ali Hosseini [ID][c]

[a] PhD of Environmental engineering-EnviroWise Research Associate Limited, Canterbury, New Zealand

[b] Professor of environmental engineering, Tehran university, Tehran, Iran

[c] PhD of Chemical engineering, Process and Reliability Engineer at BC Hydro, Iran

Abstract

Lack of proper municipal solid management in the Northern provinces of Iran has led to damages to the natural resources, health, environment, social and economic conditions. Construction of solid waste processing plants such as compost and incineration, ignoring essential elements in waste management, cannot be as a successful strategy to solve the solid waste problems. Integrated management as a suitable and well-proved solution in many developed countries was proposed for Mazandaran province as a more reliable strategy to replace the existing conditions. In this paper, the results of study conducted for Amol and Noor region have been analyzed. Minimizing waste production, maximizing recycling and reuse, processing organic waste through digestion or composting process, producing refusing derived fuel (RDF) and using it in the waste incineration plants or Neka cement plant and finally disposing less than 10% of the waste in landfill is the proposed solution to improve the existing waste conditions. Implementing the proposed integrated management over a period of 20 years will lead to preventing from economic and environmental damages due to the loss of valuable natural resources and the release of various pollutants from landfills which is evaluated to be equivalent of about 28 billion dollars also, saving resources and energy estimated to be about 38 billion dollars. © 2017 Journals-Researchers. All rights reserved. (DOI:**https//doi.org/10.52547/JCER.5.3.15**)

1. Note

In many developed as well as developing countries, poor management on produced solid waste has caused to serious environmental challenge[1, 2]. However, global environmental and energy concerns make waste management studies necessary even for small towns[3]. The concept of "zero waste management" is a globally approved strategy to solve the waste

_____

* Corresponding author. Tel.: +989123111147; e-mail: envhosseini@gmail.com.

problems. In this strategy, waste is considered a valuable source of materials produced in the natural resources consuming process [18]. The main task of the municipal solid waste management is to minimize the adverse environmental effects of waste generation by minimizing waste production, encouraging the reuse of the usable part of waste and recycling and producing new waste products[2]. Key parameters in waste management are: rules, tax rate, actual available information, available credit, financial transparency, cost-benefit of the project, environmental parameters, project technical conditions and access to the technology, knowledge and expertise [4].

Integrated waste management is one of the most important requirements of the European Union in the field of waste management to let Turkey to join the Union. In order to implement integrated waste management, Turkey needs to implement important measures such as decreasing waste production, increasing recycling of recyclable materials, processing of organic materials with compost or digestion processes, energy recovery by burning material residues and land filling for residual waste (15).

In some of the Southeast Asian countries, in order to create integrated waste management to minimize waste disposal, the following steps have been taken as zero waste achievement topics: improving public behavior, awareness and education, minimizing and prevention of waste generation, waste recycling and compost production, conversion of waste to energy and improving the landfill conditions and post-landfill care [16]. The results of a study on different waste management scenarios in Tehran, Iran, indicated that the least Green House Gases (GHGs) emissions occurs when 50 percent of MSW burn in waste to energy plant, 20 percent recycle and use of sanitary landfill for rest of them[5]. Emission of GHG could be decrease via the diversion of plastic waste by implementation of zero waste strategies [14].

Quantifying the output of each MSW strategy makes it possible to compare them more logically[7]. Thus, the outcomes of each MSW scenarios were quantified that was performed using Waste Reduction Model (WARM), and is recommended by the EPA[8]. WARM model measures emissions in terms of metric tons of carbon dioxide equivalent (MTCO2E) or metric tons of carbon equivalent (MTCE) and energy savings in millions of BTUs. Waste generation data and recycling factors in baseline scenario are one of serious limitations in this kind of studies [14].

Mazandaran province with daily MSW production of about 3000 tons is equipped with 3 recycling and compost production units. Total capacity of these plants is 750 tons per day (TPD). Nowshahr incineration plant with daily capacity of 200 tons of mixed MSW and Sari incineration with 450 TPD capacities are other projects being completed in the province. Noor and Ghaemshahr compost projects with a total capacity of 750 tons per day are in the early stages of completion. Waste management studies in Babolsar and Amol regions are being finalized[9].

The purpose of this paper is to compare the current conditions of MSW management in Noor and Amol regions with the proposed scenario in terms of technical, economic and environmental parameters by WARM. This article is part of the studies conducted for the governorate of Mazandaran with the aim of achieving zero waste, which was conducted during 2020 and 2021.

2. Methodology

This research includes the following steps: 1. Study and analysis the quality of the waste in the area, 2. Defining the possible scenarios based on the existing conditions, 3. Calculating the amount of carbon emissions in each proposed scenario using WARM software, 4. Economic review of the implementation of each scenario and 5. Summarizing the results and proposing the best scenario

2.1. Study area

Amol, as a waste management region of Mazandaran province, Iran, includes the county of Amol with a population of about 402 thousand people and county of Mahmoud Abad with a population of nearly 100 thousand people. The generated waste in this area is estimated around 350 TPD tons per day. Most of this waste is disposed directly in the Amol landfill. In Amol county geographical and environmental constraints to find a suitable place for
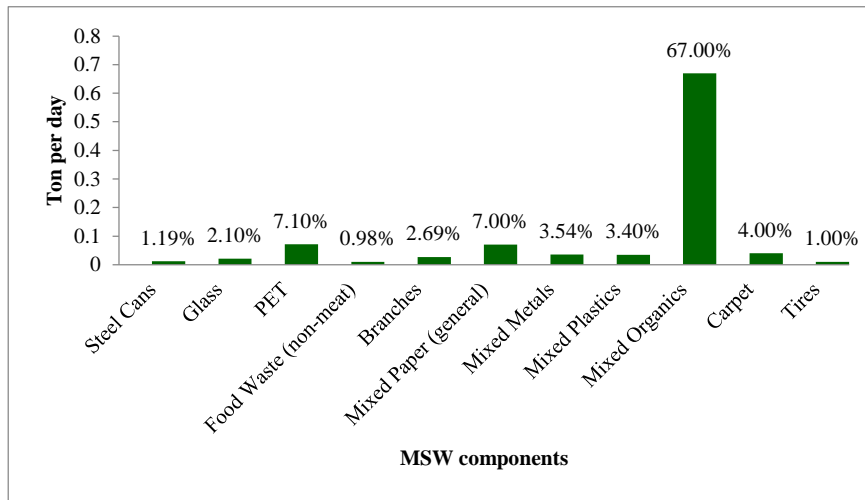
Figure 1. Average composition of MSW in Amol-Noor rejoins

the construction of waste processing facilities is one of the main concerns in MSW management.

MSW generation in Noor county, located 45 km away from Amol, is about 150 TPD. In order to enhance the economic, technical and environmental justification of the projects, it is suggested that Amol and Noor regions with a total capacity of 600 tons per day be managed together [9].

2.2. Waste quality

The results of analysis show that about 70% of the MSW in the area are degradable organic matters, including kitchen waste, twigs and other organic matter. Mixtures of PET and plastic are the second highest fraction in the analysis followed by the mixture of paper and cardboard (Figure 1).

The high percentage of polymer and plastic materials in the MSW stream is significant, indicating the massive use of disposable containers and plastic bag in this area. Therefore, by implementing waste generation reduction projects, source separation and recycling, landfill costs will be reduced and landfill operational life will be increased. Due to the high percentage of the organic matters in the MSW, the use of biological processes such as compost and digestion can be a proper option for processing the organic part of MSW.

2.3. Define different scenarios based on the existing conditions

The results of this study show that the following MSW management scenarios can be presented for the region[9]:

Scenario #	Proposed MSW management strategy
1- Based line waste management	Separation of 1.47% recyclable waste by illegal group and dumping rest of MSW in a non-engineered landfill.
2- Implementation of integrated waste management	waste reduction projects at the sources, utilization of recycling, anaerobic digestion of organic waste and RDF units and implementation of sanitary landfill

Keep going with the current condition is the most available choice, however in terms of technical and economical consideration, using of mix incineration of MSW is completely an unjustifiable and unreliable option. Therefore, in the continuation of this article, only scenarios 1 and 2 will be considered.

2.4. Calculating carbon emissions in each scenario by WARM software

Evaluation indicators that are used to quantify various waste management activities, including waste reduction percent, recycling rate, composting rate, landfilling, incineration and digestion in the form of energy saving and reducing greenhouse gas (GHG) emissions. This software calculates the amount of GHG emissions and the amount of energy saved from recycling for the current waste management conditions and proposed scenarios. Another word, the impact of each proposed scenario on the waste management is calculated and quantified in the form of emissions reduction and energy savings. Thus, according to the results, the efficiency of that strategy on waste management was determined.

The Environmental Defense Fund (EDF) has an initial estimate of the social cost of carbon emissions of $50 per ton, which is expected to be lower than the actual effects of carbon emissions (Harward, 2015). According to the studies conducted by the EPA in 2017, the real costs of carbon emissions are increasing every day because the harmful effects of carbon emissions in the coming years are far more destructive than their effects in previous years, in other words, its

impact multiplies over time [13]. But according to the US Congressional Research Service, $25 per ton of carbon emissions is taxed in 2018 for emitting units [17]. According to a study by the US government, $37 is considered too low to compensate for the social cost of carbon emissions, and $220 per ton is a good number[11]. In this project the cost of carbon emission was consider $50 per ton of CO_2.
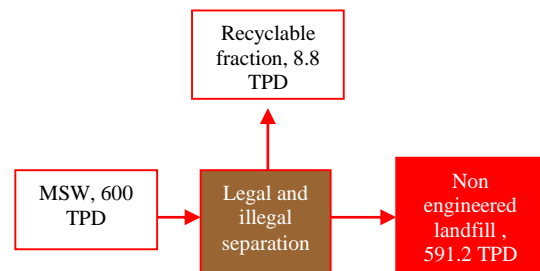

Figure 2. MSW stream for the first scenario

3. Results and discussion

3.1. The first scenario (Baseline waste management)

Table 1.

Input data to WARM for scenario 1

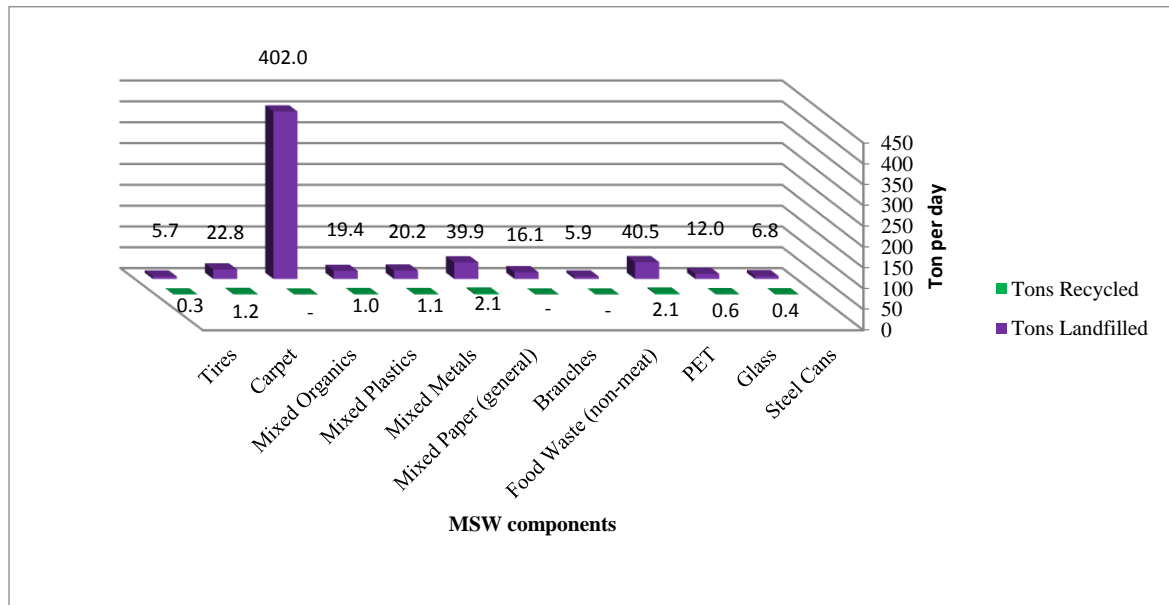| Scenario 1 - Land Filling (Ton per day)						
Material	**Tons Recycled**	**Tons Landfilled**	**Tons Combusted**	**Tons Composted**	**Tons Anaerobically Digested**	**Tons Generated**
Steel Cans	0.4	6.8	0.0	0.0	0.0	7.1
Glass	0.6	12.0	0.0	0.0	0.0	12.6
PET	2.1	40.5	0.0	0.0	0.0	42.6
Food Waste (non-meat)	0.0	5.9	0.0	0.0	0.0	5.9
Branches	0.0	16.1	0.0	0.0	0.0	16.1
Mixed Paper (general)	2.1	39.9	0.0	0.0	0.0	42.0
Mixed Metals	1.1	20.2	0.0	0.0	0.0	21.2
Mixed Plastics	1.0	19.4	0.0	0.0	0.0	20.4
Mixed Organics	0.0	402.0	0.0	0.0	0.0	402.0
Carpet	1.2	22.8	0.0	0.0	0.0	24.0
Tires	0.3	5.7	0.0	0.0	0.0	6.0
Total	**8.8**	**591.2**	**0.0**	**0.0**	**0.0**	**600.0**

Figure 3. landfilled and recycled materials in scenario 1(baseline MSW management)

Table 2.

GHG Emissions from Baseline Waste Management (Scenario 1)

Material	Tons Recycled	Tons Landfilled	Tons Combusted	Tons Composted	Tons Anaerobically Digested	Total MTCO₂E
Steel Cans	0.36	6.78	0	0	0	(0.50)
Glass	0.63	11.97	0	0	0	0.08
PET	2.13	40.47	0	0	0	(1.51)
Food Waste (non-meat)	0	5.88	0	0	0	8.20
Branches	0	16.14	0	0	0	4.25
Mixed Paper (general)	2.10	39.90	0	0	0	50.19
Mixed Metals	1.06	20.18	0	0	0	(4.18)
Mixed Plastics	1.02	19.38	0	0	0	(0.63)
Mixed Organics	0	402.00	0	0	0	333.24
Carpet	1.20	22.80	0	0	0	(2.34)
Tires	0.30	5.70	0	0	0	0.01
Total	8.8	591.2	0	0	0	386.81

The first scenario deals with current waste management activities. Figure 2 shows the waste generated area in the current conditions.

Based on the ongoing activities in the region, it is estimated that about 5% of recyclable materials, which is equivalent to 8.8 tons per day, is separated by legal and illegal groups. Rest of the waste, over 590 tons per

day, is disposed in semi-engineered landfill. The input data to WARM software for Scenario 1 (existing conditions) are presented in Table 1 and Figure 3.

The output results of WARM software based on the amount of greenhouse gas emissions for different activities in baseline waste management are shown as table 2. Daily amount of GHG emissions form current MSW management is 386.81 MTCO$_2$E.

3.2. The second scenario (Alternative scenario)

According to the successful waste management project experiences of countries with a culture similar to Iran, the second scenario based on implementation of integrated waste management is defined as following [9]:

• Implementing a plan to reduce waste generation at the sources [7]

• Construction of transfer stations to cover 100% of the cities and villages of the region

• Site selection for construction of projects according to environmental organization criteria

• Use of biological processes such as anaerobic digestion to process organic waste

• Production of RDF from non-recyclable part with high energy content and transfer to the cement production plant or Sari incinerator plan.

• Update the existing landfill

Accordingly, the waste flow in the second scenario will be as shown in Figure 4.

Regarding to MSW characteristics and our previous filed study results, in scenario 2, around 130 TPD of MSW will be reduced due to reduced waste generation and source separations. Production of 2 to 3 megawatts of electricity, average 2.5 MW, by anaerobic digestion plant, daily production of about 65 tons of high-quality organic fertilizer and daily production of around 50 tons of RDF that can be used in Nowshahr or Sari incineration plants or Neka cement plant, are other outputs of this scenario. Other studies confirm this scenario for achieving to waste to energy and waste minimization [15]. Covert MSW to energy leads to reduces the GHG emissions and other environmental benefits [14]. In this scenario, the amount of landfill is reduced to less than 40 tons per day. Prevention of GHG emission of 395.95 MTCO$_2$E is another achievement of alternative scenario. Table 3 shows the input data and output results of WARM software, the amount of greenhouse gas emissions for different activities in Scenario 2.
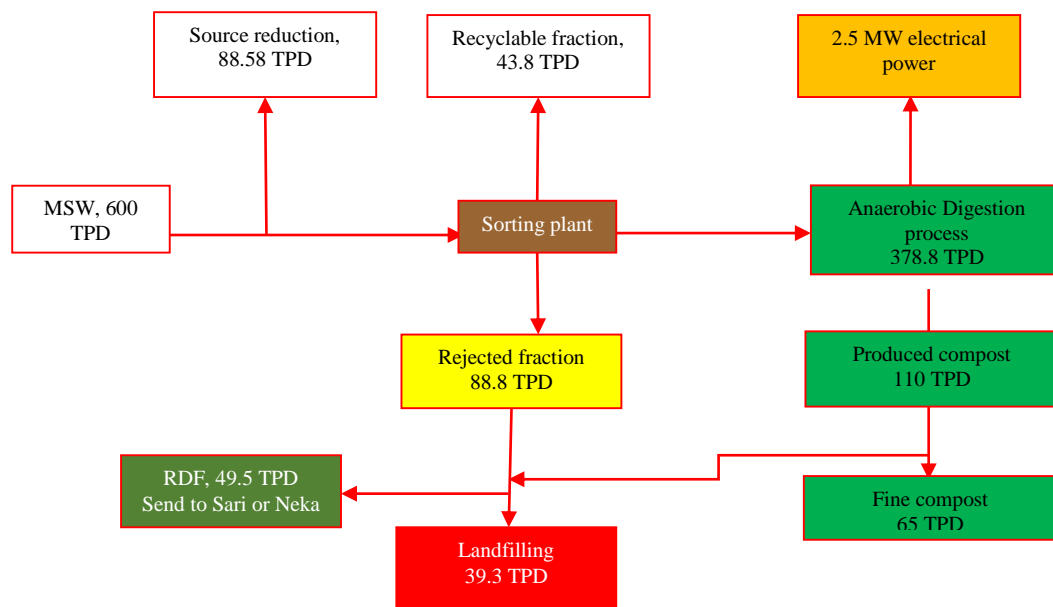

Figure 4. Waste stream in the second scenario for Amol-Noor region

Table 3.

GHG Emissions from scenario 2 (alternative waste management scenario) (TPD)

Material	Tons Source Reduced	Tons Recycled	Tons Landfilled	Tons Combusted	Tons Anaerobically Digested	Total MTCO$_2$E
Steel Cans	3.6	2.1	0.7	0.7	-	-15.92
Glass	6.3	3.8	1.3	1.3	-	-4.29
PET	21.3	12.8	4.3	4.3	-	-55.90
Food Waste (non-meat)	0.6	-	0.6	0.6	4.1	0.09
Branches	-	-	1.6	1.6	12.9	-2.80
Mixed Paper (general)	21.0	8.4	4.2	8.4	-	-156.22
Mixed Metals	10.6	6.4	2.1	2.1	-	-69.08
Mixed Plastics	10.2	6.1	2.0	2.0	-	-23.34
Mixed Organics	-	-	20.1	20.1	361.8	-11.95
Carpet	12.0	2.4	2.4	7.2	-	-43.62
Tires	3.0	1.8	0.0	1.2	-	-12.91
Total	**88.58**	**43.8**	**39.3**	**49.5**	**378.8**	**-395.95**

3.3. Comparison of greenhouse gas emissions

Comparison of greenhouse gas emissions in the scenarios 1 and 2 for Amol-Noor region is given in the following tables.

Table 4.

Quantitative evaluation of waste scenarios in Amol-Noor region

Indicator	Scenario 1	Scenario 2
GHG emission (MTCO$_2$E)	386.81	-395.95
GHGs emissions in metric tons of carbon dioxide equivalent (MTCO2E)		

Negative numbers indicate a reduction in greenhouse gas emissions

Under the current conditions of waste management in Amol-Noor region, more than 386 tons of greenhouse gases are daily released into the air. However, after the implementation of the second scenario, in addition to preventing the emission of greenhouse gases released in scenario one, the emission of more than 395 tons of greenhouse gases will be reduced due to material recycling that prevents the extraction and processing of natural resources. The study that carried out on Malaysian MSW management improved that the carbon emission factor of dumping area of MSW was highest, however it was lowest for recycling of materials [12].

3.4. Economic analysis of scenarios 1 and 2

A comparison of revenues, expenditures and the amount of greenhouse gases produced by implementing scenarios 1 and 2 based on the year of the study (2020) is shown in Table 5. As this table shows, for Amol-Noor region with about 600 TPD of MSW , the required investment for Scenario 1 is about USD 466777 as initial investment and USD 466776.92 annually for sanitary landfill operation, while implementation of Scenario 2 requires an initial investment of more than USD 20546192 (more than 40 times of Scenario 1) and its operating cost is estimated more than USD 1438233 (more than 3 times of Scenario 1).

Many of studies were proved that the most sustainable and short-term solution is recycling of materials[7], so, revenues from material recycling in Scenario 1 can cover the cost of sanitary landfilling, and in Scenario 2, revenues from project implementation can cover the costs of project operation. Of course, in this study, the assumption of financing the construction of the projects is gratuitous

by the government. Obviously, if the initial investment of the project is made by the private sector, the investment model will be completely change and parameters such as bank interest, investment profit, etc. must be considered.

Table 5.

Technical and economic study of the proposed scenarios for Amol-Noor regions

Item		Scenario 1	Scenario 2
Execution costs of recycling unit, USD	Recycling Unit	-	830769.23
	Anaerobic digestor	-	15384615.38
	Composting unit	-	3100038.46
	RDF production	-	1230769.23
	Incineration plant	-	-
	landfilling	466776.92	36500
Emissions (MTCO$_2$E)		386.81	-395.95
Products	Recycling (TPD)	8.8	132.38
	Compost (TPD)	-	65
	RDF (TPD)	-	49.5
	Landfilling (TPD)	591.2	39.3
	Electricity (MW)	-	2.5
Annual Income, USD		494153.85	9884607.69
Initial investment, USD		466776.92	20546192.31
Annual Operational cost, USD		466776.92	1438233.46

If the losses of $50 per ton of carbon emissions is considered, based on the investment data presented in Table 5, the total costs and Revenues by implementing scenarios 1 and 2 for a period of 20 years are shown in Table 6.

According to the Table 6, implementation of Scenario 1 in a period of 20 years, causes more than 141 million USD of economic and environmental damages due to the waste of resources and various pollutants emissions from landfills. While implementation of Scenario 2, in a same period leads to saving of about 293 million USD by preserving in resources and energy through implementation of integrated waste management.

Table 6.

Costs and incomes of Amol-Noor proposed scenarios for a period of 20 years

Parameters for 20 years operation	Scenario 1	Scenario 2
Total investment, USD	466776.92	20546192.31
Total Incomes, USD	9883076.923	197692153.8
Operational Costs, USD	9335538.462	28764669.23
Environmental impact costs, USD	141185650	-144521750
Sum, USD	-141104888.46	292903042.3

4. Conclusion

Municipal solid waste issue in the northern provinces of Iran has been a serious concern of national and regional government for many years. Lack of a clear roadmap to solve the MSW problem and also lack of an independent organization to prepare and implement waste management projects, most of the waste problems remained unsolved. Implementing integrated waste management with the aim of minimizing waste production, increasing recycling, organic waste processing by anaerobic digestion, RDF production to reduce the risk and costs of incinerator construction and decreasing waste disposal could be a proper solution to solve the waste problem of the northern provinces of Iran. The most sustainable and short-term solution is recycling of materials. Allocation of sufficient grants by the government to implement integrated waste management can provide sufficient technical, environmental and economic justification for the private sector to enter and solve the problem of waste in different parts of the country.

Analysis of solid waste management scenarios using the WARM model: Case study. Journal of Cleaner Production, Volume 345, p. 130687.

References

[1] Maity, S., 2018. Importance of municipal solid waste management. International Journal of Advanced Engineering Research and Science, Volume 5, pp. 2349-6495

[2] Collins O. Ugwu, C. G. O. P. A. O. N. A. C. M., 2021. Waste reduction and utilization strategies to improve municipal solid waste management on Nigerian campuses. Fuel Communications, Volume 9, p. 100025.

[3] Gulgun Kayakutlu, T. D. M. K. A. A. Y. S., 2017. Scenarios for regional waste management. Renewable and Sustainable Energy Reviews, Volume 74, pp. 1323-1335.

[4] Klavenieks, K. & Dezne, K. P., 2017. Optimal strategies for municipal solid waste treatment – environmental and socio-economic criteria assessment. Energy Procedia, Volume 128, pp. 512-519.

[5] Abtin Maghmoumi, F. M. E. H., 2020. Environmental and economic assessment of sustainable municipal solid waste management strategies in Iran. Sustainable Cities and Society, Volume 59, p. 102161.

[6] Ozturk, M., 2015. The Roadmap of Turkey on Waste Management. Waste management, 5(12).

[7] Pâmela de Medeiros Engelmann, V. H. J. M. d. S. P. R. d. R. G. H. A. d. S. R. V. L. J. E. A. d. L. M. J. R. P., 2022.

[8] EPA, 2019. [Online] Available at: WWW.EPA.gov/warm/versions-waste-reduction-model-warm [Accessed 2019].

[9] Hosseini, S. M. M. N., 2021. Mazandaran integrated solid waste management, Sari, Iran: Mazandaran Science Technology Park.

[10] Harward, P., 2015. Expert consensus on the economics of climate change, Institute for policy integrity. s.l.:New York University.

[11] Moore, F. C., 2015. Temperature impacts on economic growth warrant stringent mitigation policy. Natural Climate Change , Volume 5.

[12] Zheng Ting Chew, Z. X. H. K. S. W. P. Y. L., 2022. Integrating greenhouse gas reduction and waste policy targets to identify optimal waste treatment configurations via Carbon Emission Pinch Analysis. Process Safety and Environmental Protection, Volume 160, pp. 661-675.

[13] EPA, 2017. [Online] Available at: . https://19january2017snapshot.epa.gov/climatechange/social-cost-carbon_.html

[14] Joshua R. Castigliego, A. P. C. J. C. M. J. W., 2021. Evaluating emissions reductions from zero waste strategies under dynamic conditions: A case study from Boston. Waste Management, Volume 126, pp. 170-179.

[15] Klavenieks, K. & Dezne, K. P., 2017. Optimal strategies for municipal solid waste treatment – environmental and socio-economic criteria assessment. Energy Procedia, Volume 128, pp. 512-519.

[16] Pacific, U. R. R. C. f. A. a. t., 2010. Municipal Waste Management Report: Status-quo and Issues in Southeast and East Asian Countries.

[17] Services, C. R., 2019. Attaching price to greenhouse gas emissions with a carbon tax or emissions fee: consideration and potential impact, s.l.: s.n.

[18] Zaman, A. U., 2014. Identification of key assessment indicators of the zero waste management system. Ecological Indicators, Volume 36, pp. 682-693.

Investigating the Mechanical and Durability Properties of Geopolymer Concrete Based on Granulated Blast Furnace Slag as Green Concrete

Mohammadhossein Mansourghanaei [a*]

[a] Ph.D. in Civil Engineering, Department of Civil Engineering, Chalous Branch, Islamic Azad University, Chalous, Iran

Abstract

Geopolymer concretes (GPCs) are known as green, environmentally friendly, sustainable concretes in the development of the structural industry with superior mechanical performance and durability compared to ordinary Portland cement concrete (OPCC). This type of concrete emits less CO_2 than OPCC and aims for efficient waste management while reducing environmental impacts. In this experimental research, 5 mixed designs were made of GPC based on granulated blast furnace slag (GBFS), which contains 0-8% Nano silica (NS) and 1-2% polyolefin fibers (POFs). A mixed design was also made of OPCC to compare with GPC. The tests of compressive strength, tensile strength, drop weight impact (DWI), Ultrasonic Pulse Velocity (UPV), water permeability and microstructural examination by scanning electron microscope (SEM) images and X-ray fluorescence (XRF) spectroscopy were performed on concrete samples and the results were analyzed and compared. The results obtained in this laboratory research, while overlapping with each other, indicate the superiority of mechanical properties and durability of GPC compared to OPCC. © 2017 Journals-Researchers. All rights reserved. (DOI:**https//doi.org/10.52547/JCER.5.3.24**)

Keywords : Geopolymer Concrete (GPC), Granulated Blast Furnace Slag (GBFS), Nano Silica (NS), Polyolefin Fibers (POFs), Mechanical and Durability Properties.

[*] Corresponding Author. Tel: +989121712070; E-mail: Mhm.Ghanaei@iauc.ac.ir

1. Introduction

Cement is the second most consumed product (after water) in the world [1] and the third source of toxic carbon dioxide (CO_2) emissions in the atmosphere [2] and it is estimated that cement is responsible for producing 5-8% of CO_2 in the atmosphere. [2,3]. In this regard, with the production of one ton of cement, approximately one ton of CO_2 gas is released into the atmosphere [4]. On the other hand, cement production requires high consumption of energy and mineral resources [5]. These challenges have led scientists to search for alternatives such as the production of green concrete or GPC [6]. GPC are emerging as one of the building materials [7]. GPC is produced from the process of geopolymerization, in which molecules known as oligomers are combined to form covalently bonded geopolymer networks [8]. The properties of GPC are determined based on the properties of the materials used and its processing conditions [9]. In this regard, the results showed that alkaline materials and active alkali solution (AAS) are the two main factors influencing the properties of GPC [10]. Environmentally friendly, stable and structurally sound GPC can be made from industrial waste (such as GBFS), municipal waste (such as construction waste) and agricultural waste (such as rice husk ash) [11,12]. The use of these wastes in the composition of GPC will lead to efficient waste management while reducing environmental pollution. Researchers' findings have shown that the use of industrial waste materials compared to ordinary cement in the composition of GPC also reduces the cost of concrete production [13]. It has been reported that the amount of CO_2 produced in GPC is lower than ordinary Portland concrete (OPC) [7,14-18]. On the other hand, due to high compressive strength, low permeability and high resistance to acid attack, GPCs are a suitable alternative to OPCC in the construction of structures [8]. In the production of GPC, active alkali solutions such as potassium hydroxide (KOH), sodium hydroxide (NaOH), potassium silicate (K_2SiO_3) or sodium silicate (Na_2SiO_3) are needed for the geopolymerization of aluminosilicate precursors [19]. In this regard, the most commonly used combined active alkali solution in GPC is the use of sodium hydroxide (NaOH) and sodium silicate (Na_2SiO_3), which have been used in several studies [20-22]. Hydrated gels are the main factor in creating bond and strength in the hardened GPC structure. In GPC based on GBFS, the production of hydrated gels such as C-S-H, N-A-S-H and C-A-S-H is high in the geopolymerization process, and the largest volume of production belongs to C-S-H gel. Studies show that C-A-S-H gel is formed in the interfacial transition zones (ITZ) in the geopolymerization process of GPC based on GBFS, which helps to increase the compressive strength of this type of concrete compared to OPCC slow [23]. The amount of porosity and pores in the microstructure of GPC is less than that of OPCC, and this is one of the main factors of the superiority of mechanical properties and durability in GPC compared to OPCC. In this regard, the microscopic morphology of concrete samples with SEM images of the microstructure of GPC based on GBFS show more microstructure than OPCC (which has large pores) [6,23]. On the other hand, microstructure studies on GPC show better characteristics of ITZ compared to OPCC [24]. Also, studies have shown that increasing the curing temperature in GPC based on GBFS improves the laboratory results [25]. Industrial wastes such as GBFS, which often have unknown uses, are usually dumped in landfills, which lead to environmental pollution [26]. It has been estimated that for each ton of steel production, about 400 kg of steel furnace slag including GBFS and basic oxygen furnace slag (BOFS) are produced. GBFS contains siliceous (Si) and aluminate (Al) materials, the different amounts of which are used in the composition of concrete, can have a positive effect on the speed of the geopolymerization process [26]. On the other hand, GBFS helps in forming a larger volume of hydrated gels (compared to OPC) such as C-S-H in the composition of GPC [27]. Research has shown that the mechanical performance and durability of GPC based on GBFS is beyond that of OPCC [28-30]. The use of nanomaterials rich in aluminate and silicate particles in the composition of GBFS GPC leads to the improvement of mechanical properties in this type of concrete [12,31,32]. This issue is mostly due to the increase in the speed of the geopolymerization process and the greater participation of nanoparticles in the chemical reaction process in GPC [33]. In this regard, the addition of NS to the composition of GPC improves the mechanical properties of this type of concrete [34]. The use of fibers in the composition of concrete improves the mechanical properties and durability of concrete [35,36]. In this regard, the use of fibers improves the tensile strength of GPC [37], but the excessive use of fibers in the composition of

concrete causes a decrease in the mechanical properties of this type of concrete [38]. The type of fibers used clearly affects the compaction of concrete according to its density [39]. Research shows that the use of fibers in GPC improves the durability of concrete in the long term [40]. On the other hand, fibers improve tensile strength, increase energy absorption capacity, toughness and ductility in GPC [41]. In this laboratory study, increasing the mechanical properties and durability of GBFS NS and POFs is one of the innovative goals. On the other hand, according to the research of others, helping the healthy environment by reducing CO_2 emissions from conventional cement production, is another goal in this research.

2. Experimental Program
2.1 Materials

In this experimental study, the OPC type II with a 2.35 g/cm^3 of specific weight according to standard En 197-1 and the GBFS was used in powder form with the density of 2.75 g/cm^3 according to ASTM C989/C989M standard. The chemical properties of these materials are indicated in Table 1. The NS particles made up of 99.5% SiO_2 with an average diameter in the range of 15 to 25 nm were used. Crimped POFs according to ASTM D7508/D7508M standard, 30 mm in length, were also used, whose physical properties are shown in Fig. 1. The used fine aggregates were natural clean sand with a fineness modulus of 2.95 and a density of 2.75 g/cm^3, and the coarse aggregates were crushed gravel with a maximum size of 19 mm and a density of 2.65 g/cm^3 according to the requirements of the ASTM-C33. In this research, thermal curing of GPC has been done at 60 ℃ for 48 hours in an electric furnace under 80±3% relative humidity. In this regard, research has shown that thermal curing of GPC based on GBFS leads to improvement of mechanical properties and durability in concrete [28,16].

2.2 Mix Design

For accurate investigation, six mixture designs were considered, according to ACI 211.1-89 standard. For GPC, as in other articles [28,42], a OPCC mixing scheme was used. The first sample included a regular concrete containing Portland cement where the water to cement ratio has considered to be constantly 0.45. Five other samples include GPC with different NS

and POFs. The GPC samples are generally categorized into two groups: the first group lacks POFs with the NS amount of 0-8%. The second group contains 8% of NS, where the POFs are used in these designs in the form of 1 and 2 percent. In order to achieve the same performance in each mixture design and obtain a slump of about 20 ±100 mm, we have used normal polycarboxylate based superplasticizers. Besides, 202.5 kg/m^3 of the alkaline solution is used in this case. The used alkaline solution is a combination of NaOH and Na_2SiO_3 with the weight ratio of 2.5, utilized with the mixture specific weight of 1483 kg/m^3 and the concentration of 12 M. The conducted studies indicate that due to the significant level of C-S-H formation when utilizing Na_2SiO_3, using a combination of NaOH and Na_2SiO_3 increases the compressive strength compared to single employment of CaOH [43]. The samples mixture design is indicated in Table 2.

Tensile Strength (N/mm²)	>500
Length (mm)	30
Diameter (mm)	0.8
Elasticity Modulus (GPa)	>11
Bulk Density (g/cm³)	0.910

Fig. 1. Physical Properties of the POFs

Table 1
Chemical Compositions of Materials (%)

Component	GBFS	OPC
SiO_2	29.2	21.3
Al_2O_3	19.4	4.7
Fe_2O_3	5.8	4.3
CaO	38.6	62.7
MgO	2.8	2.1
SO_3	2.6	2
K_2O	0.1	0.65
Na_2O	0.2	0.18
TiO_2	0.6	-
Free Cao	-	1.12
LOI	0.3	1.84

Table 2
Details of the Mix Designs

	Mix ID	OPC	GBFS	Water	AAS	NS	Coarse Aggregates	Fine Aggregates	POFs	Super Plasticizer
							(Kg/m^3)			
1	OPCC	450	0	202.5	0	0	1000	761	0	6.75
2	GPCNS0POF0	0	450	0	202.5	0	1000	816	0	6.75
3	GPCNS4POF0	0	432	0	202.5	18	1000	767	0	7.8
4	GPCNS8POF0	0	414	0	202.5	36	1000	718	0	8.3
5	GPCNS8POF1	0	432	0	202.5	36	1000	672	24	8.6
6	GPCNS8POF2	0	432	0	202.5	36	1000	646	48	9

2.3 Test Methods

After fabricating the samples, for better curing and increasing the resistance properties, the samples were placed in an oven at 60 °C with a thermal rate of 4.4 °C/min for 48 h. In this study, the compressive strength tests were performed on 10-cm^3 cubic specimens based on BS EN 12390. to determine the tensile strength of the cylindrical specimens (15 cm in diameter and 30 cm in length), the splitting tests were conducted based on ASTM C496. The concrete's resistance to dynamic loads (impacts) was measured using the drop weight hammer test according to the report by the ACI 544-2R committee. This test was conducted with repeating impacts on disks with a diameter of 15 cm and a height of 63.5 cm. The UPV tests were conducted according to ASTM C597 using a non-destructive ultrasonic electronic apparatus, PUNDIT MODEL PC1012, with an accuracy of ±0.1 μs for a transformator with a vibrational frequency of 55 kHz and a movement time accuracy of ±2% for the distance. According to EN 12390-8, the water permeability tests were performed on 150×150×150-mm^3 cubic specimens with a water pressure of 50±500 kPa on a circular area with a diameter of 75 mm on one of the surfaces for 72 hours. In this article, the tests of compressive strength, tensile strength, DWI, UPV, water permeability in concrete at the curing age of 7, 28 and 90 days were performed. XRF analysis at 7 days curing age and SEM analysis at 90 days curing age were performed on concrete samples.

3. Results and Discussion

3.1 Results of the Compressive Strength Test

The results of the compressive strength test of concrete samples in this laboratory research are shown in Figure 2. Figure 3 shows the concrete samples in each mix design after performing the compressive strength test at the age of 90 days curing. Based on the results, it can be seen that increasing the curing age in the concrete of each design has led to an improvement in compressive strength. This issue is due to the progress of the chemical reaction process and the production of a higher volume of hydrated gels such as C-S-H in the concrete composition at the same time as the age curing of the concrete increases [44].

By increasing NS particles in GPC, the compressive strength of concrete has improved. This is due to the increase in the rate of polymerization and the production of more volume of hydrated gels in the composition of GPC [33]. The increase of POFs in the composition of GBFS-based GPC has led to a drop in the compressive strength results of this type of concrete. This issue can be due to the type of fibers used and the improper bonding of fibers with geopolymeric mortar in the interfacial transition zone (ITZ). Design GPCNS8POF0 is the best plan in terms of achieving compressive strength, so that at the age of 90 days curing, it has achieved a 33% better result than design OPCC and 29% better than design GPCNS0POF2.

3.2 Results of the Tensile Strength Test

Figure 4 shows the results of the tensile strength test in this laboratory research. Figure 5 includes the concrete samples of all the mixed designs after the tensile strength test. Based on the results, increasing the age of concrete curing has led to improved results in all designs. In this regard, OPCC with 93% increase in GPC design GPCNS4POF0 with 72% increase was a step forward. In GPCs, the addition of NS has led to the improvement of tensile strength results in concrete, in this regard, at the age of 90 days of curing (as the best curing age), design GPCNS8POF0 with 8% NS obtained 15% higher tensile strength than design GPCNS0POF0 without NS. The addition of up to 2% POFs in the GPC mixture led to the improvement of the tensile strength test results in this research. So that at the age of 90 days, design GPCNS8POF2 (containing 2% POFs) obtained 8% more tensile strength than design GPCNS8POF0 (without POFs). This issue is mostly due to the proper bonding of POFs in the GPC composition under Brazilian tensile test loading [45,46]. The findings of scientists have shown that the use of different types of fibers such as natural kenaf [47] and glass fibers [48] in the composition of GPC leads to the improvement of tensile strength in this type of concrete.

Fig. 3. Concrete Sample in Compressive Strength Test
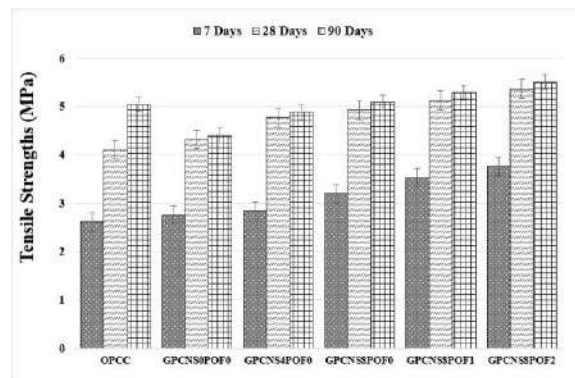
Fig. 4. The Tensile Strengths of the Specimens

Fig. 2. The Compressive Strengths of the Specimens
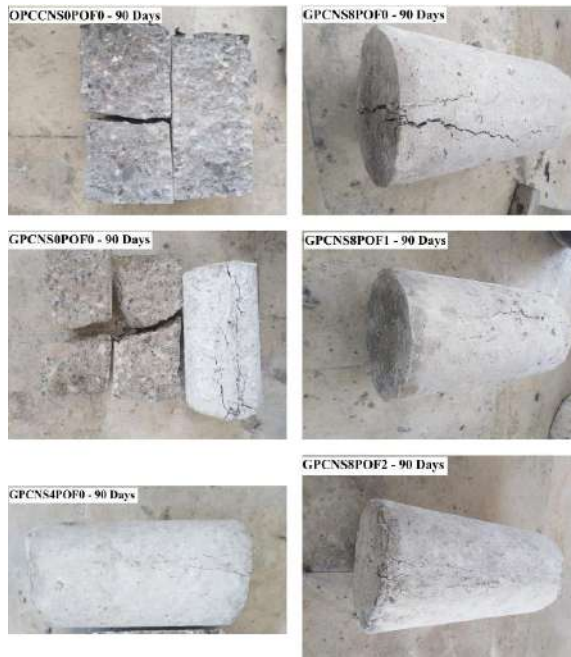
Fig. 5. Concrete Sample in Tensile Strength Test

3.3 Results of the DWI Test

The results of the impact test using the drop weight method under the initial impact energy for the occurrence of the initial crack (E_1), the impact energy of the final crack (E_2) and the flexibility index (E_2/E_1) of the concrete samples of all designs at the age of 90 days and at the ambient temperature (21-25 ℃) based on Joule is shown in the diagram of Figure 6. Figure 7 shows the device for performing the DWI test. According to the results, it can be seen that the impact energy of breaking (E_2) the concrete sample in all designs is more than the impact energy for the initial crack (E_1). The initial and final energy values for cracking and failure of the OPCC sample were lower than the corresponding values in all GPC designs. The addition of POFs up to 2% to the GPC composition led to the improvement of the resistance of concrete samples against the DWI. So that in design GPCNS8POF2, the amount of initial energy (E_1) increased by 30% and final energy (E_2) by 3.4 times compared to design GPCNS8POF0. In this regard, the amount of initial energy in design GPCNS8POF2 concrete was increased by 2.3 times and the final energy was increased by 7 times compared to OPCC. Flexibility index (E_2/E_1) in GPC samples improved by increasing the amounts of NS

and POFs. The findings of other researchers show that GBFS based GPCs have better impact resistance than OPCCs [49]. Also, in GPCs, the addition of fibers leads to the improvement of concrete resistance against impact loads [30]. The use of other types of fibers, such as in the composition of GPC, increases the resistance of this type of concrete against impact loads [50].
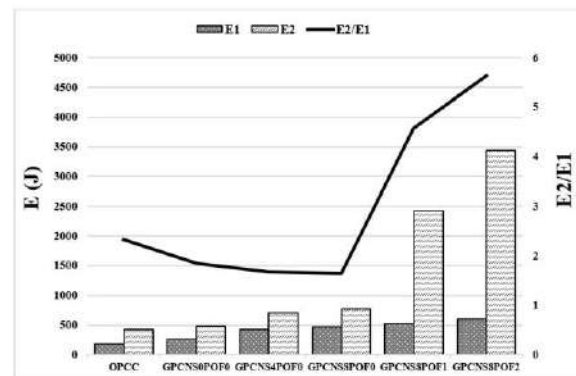
Fig. 6. The Impact of the Specimens

Fig. 7. DWI Test Machine

3.4 Results of The UPV Test

Figure 8 shows the results of UPV test on concrete samples in this research. Increasing the curing age in concrete due to the progress of the hydration and geopolymerization process in concrete has led to the improvement of UPV [28]. The addition of NS to the GPC composition leads to the production of more hydrated gels in concrete, and thus the amount of UPV has increased. The addition of polyolefin fibers to the GPC composition has led to a decrease in UPV results. In this regard, at the processing age of 90 days (as the best curing age), adding POFs to design 6 has led to a reduction of 12% in the results compared to design 4 (without POFs). UPV in OPCC at all ages is higher than UPV in GPC at corresponding ages. This issue is due to the appearance of microcracks during the thermal curing process in GPC, which has been effective on the UPV loss. In the diagram of Figure 8, the quality of concrete is determined based on the speed of waves passing through concrete according to the IS 13311-1 standard. In this regard, it can be seen that at the age of 7 days curing, concrete designs GPCNS0POF0 and GPCNS8POF0 have excellent quality and other designs are in good quality. At the age curing of 28 and 90 days, all concrete designs are of excellent quality.
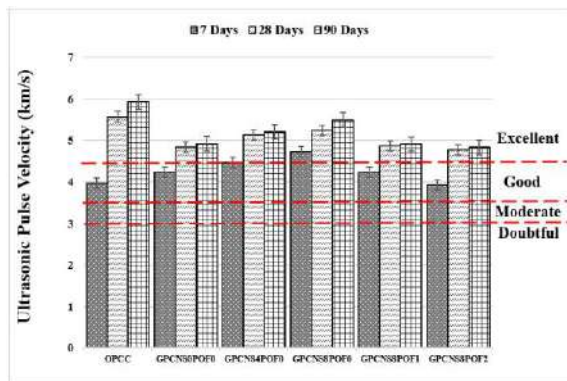
Fig. 8. The UPV of The Specimens

3.5 Results of the Water Permeability Test

The results of the water permeability test in concrete based on the depth of water penetration (in mm) in concrete are shown in the diagram of Figure 9. Based on these results, it can be seen that in each design, the depth of water penetration in concrete decreases with the increase of curing age in concrete. This issue has become harder due to the improvement of concrete density and the increase of adhesion between concrete components, which is completed by the development of the chemical process. The depth of water penetration in GPC is less than OPCC at the corresponding age, this shows the superior performance of durability in GPC compared to OPCC. The addition of NS in the composition of GPC with the improvement of the matrix of the geopolymeric structure led to a decrease in water permeability by 35% (design GPCNS8POF0 compared to design GPCNS0POF0 in 28 days of curing) in this type of concrete. The addition of POFs up to 2% in the composition of GPC led to a decrease in the depth of water penetration in this type of concrete up to 27% (design GPCNS8POF2 compared to design GPCNS8POF0). Figure 10 shows concrete samples undergoing water permeability test.
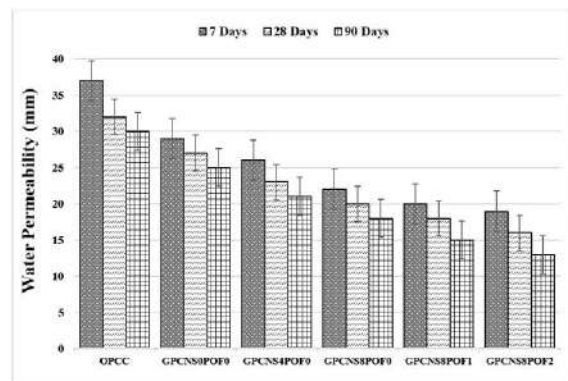

Fig. 9. The Water Permeability of The Specimens

Fig. 10. Water Permeability Test in Concrete

3.6 Results of The XRF Analysis

The results of XRF analysis of concrete samples are shown in Table 3. SiO_2, AL_2O_3 and CaO are seen as the three main elements with the highest amount in all designs. In this regard, SiO_2 amounts in plans 4, 5 and 6 (including GPC containing 8% NS) have reached the highest value (about 37%). The lowest amount of SiO_2 (27%) is found in OPCC. AL_2O_3 is found in the range of 7-8% in GPC designs, and it has reached the lowest amount (5.6%) in OPCC designs. The maximum (37%) of CaO is seen in OPCC and the maximum (26.8%) and minimum (15.3%) of CaO is seen in concrete design 2 and 5 of GPC, respectively. LOI values in all designs are in the same range (about 16%). SiO_2 and Al_2O_3 are the main elements in slag and NS (primary materials of GPC), on the other hand, CaO is also the main element of OPC in OPCC.

Table 3
XRF Test Results (%)

Component	Mix NO					
	1	2	3	4	5	6
SiO_2	27.1	19.5	32.02	36.3	37	36/8
AL_2O_3	5.6	8	6.7	7.01	7/1	6/9
CaO	37.1	26.8	23.6	15.2	15/13	15/18
Na_2O	1.1	15.1	9.01	12.8	12/64	13/01
Fe_2O_3	7.2	5.6	3.9	3.94	3/79	4
MgO	2.1	5.05	4.01	3.01	3/15	2/89
K_2O	0.9	1.01	1.01	1.05	1/12	1/14
SO_3	1.6	1.1	1.87	2.8	1/9	1/98
TiO_2	0.4	0.9	1.08	1.1	1	1/2
P_2O_5	0.1	0.1	0.14	0.1	0/139	0/153
MnO	0.1	0.4	0.65	0.6	0/64	0/71
LOI	16.4	16.04	15.9	15.7	16	15/9

3.7 Results of the SEM Analysis

The results of SEM analysis are shown in Figure 11. In the composition of ordinary concrete compared to GPC, the amount of hydrated gels (C-S-H) is seen in its lowest amount. Also, the tree structure (which shows the low density of concrete), unhydrated particles and pores in the composition of OPCC is more than the design of GPC. In GPC designs, the amount of hydrated gels has been increased by increasing the amount of NS in the designs. This process is due to the acceleration of geopolymerization activity and the production of a larger volume of hydrated gels in this type of concrete. The researchers' findings show that GPCs have superior microstructural characteristics than OPCCs [51,52]. Adding materials containing aluminosilicate sources to the composition of GPC adds its characteristics [24]. This superiority is often due to the presence of dispersed pores with very small sizes in the matrix of GPC compared to OPCC [6].
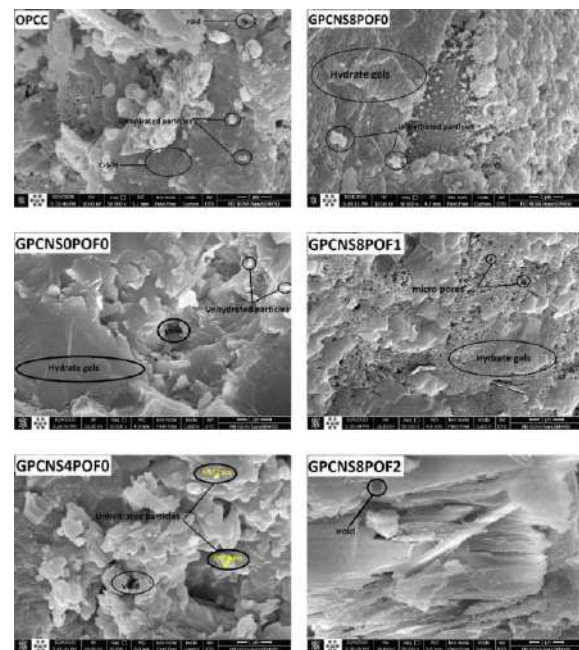

Fig. 11. SEM Image

4. Conclusions

In this article, tests of compressive strength, tensile strength, DWI, UPV, water permeability in OPCC and GPC at the curing age of 7, 28 and 90 days were performed and the results were compared and analyzed. XRF analysis at the curing age of 7 days and SEM analysis at the curing age of 90 days were performed on concrete samples and the results were evaluated. The most important results in this research are as follows.
1. Except for the UPV test, the results in all tests show the superiority of GPC over OPCC. This shows the superior performance of GBFS-based GPC compared to OPCC.

2. Due to the thermal curing in GPC that has led to microcracks, the UPV results in this type of concrete are lower than OPCC.

3. In GPC, the addition of NS has improved the results in all tests. This issue is due to the help of NS to accelerate the geopolymerization process and produce more volume of hydrated gels in the GPC matrix.

4. In GPC, the addition of POFs has improved the results in tensile strength, DWI and water permeability tests. In this regard, the addition of fibers has been appropriate to prevent crack propagation and maintain the localization of cracks.

5. The type of fiber and its connection method in GBFS-based GPC has led to a drop in results in compressive strength and UPV tests.

6. The results of XRF and SEM analysis are in agreement and overlapping with other results in this laboratory research.

References

[1] Alanqari, K., Al-Yami, A., & Wagle, V. (2022, February). Preparation of a Synthetic Geopolymer Cement Utilizing Saudi Arabian Volcanic Ash for a Sustainable Development: Method, Preparation and Applications. In International Petroleum Technology Conferenc.

[2] Vijayashankar, T., Girinath, T., Dineshkumar, S., & Saravanaganesh, S. (2022) .EXPERIMENTAL STUDY ON GEOPOLYMER CONCRETE USING HEAVY WEIGHT AGGREGATE. 04 (06).

[3] Li, L., Wei, Y. J., Li, Z., & Farooqi, M. U. (2022). Rheological and viscoelastic characterizations of fly ash/slag/silica fume-based geopolymer. *Journal of Cleaner Production*, *354*, 131629.

[4] Nishanth, L., Patil, N. N., Kumbar, N., Kaveti, S., & Kar, D. (2022). Influence of E-Coli on workability and strength characteristics of self-consolidating geopolymer concrete based on GGBFS, flyash and alccofine. Materials Today: Proceedings.

[5] Yang, S., Zhao, R., Ma, B., Si, R., & Zeng, X. (2023). Mechanical and fracture properties of fly ash-based geopolymer concrete with different fibers. Journal of Building Engineering, 63, 105281.

[6] Amin, M., Elsakhawy, Y., Abu el-hassan, K., & Abdelsalam, B. A. (2022). Behavior evaluation of sustainable high strength geopolymer concrete based on fly ash, metakaolin, and slag. Case Studies in Construction Materials, 16, e00976.

[7] Amran, M., Huang, S. S., Debbarma, S., & Rashid, R. S. (2022). Fire resistance of geopolymer concrete: A critical review. Construction and Building Materials, 324, 126722.

[8] Wong, L. S. (2022). Durability performance of geopolymer concrete: A review. Polymers, 14(5), 868.

[9] Saif, M. S., El-Hariri, M. O., Sarie-Eldin, A. I., Tayeh, B. A., & Farag, M. F. (2022). Impact of Ca^+ content and curing condition on durability performance of metakaolin-based geopolymer mortars. Case Studies in Construction Materials, 16, e00922.

[10] Feng, B., & Liu, J. (2022). Durability of Repair Metakaolin Geopolymeric Cement under Different Factors. Processes, 10(9), 1818.

[11] Shehata, N., Mohamed, O. A., Sayed, E. T., Abdelkareem, M. A., & Olabi, A. G. (2022). Geopolymer concrete as green building materials: Recent applications, sustainable development and circular economy potentials. Science of the Total Environment, 155577.

[12] Shilar, F. A., Ganachari, S. V., Patil, V. B., Nisar, K. S., Abdel-Aty, A. H., & Yahia, I. S. (2022). Evaluation of the Effect of Granite Waste Powder by Varying the Molarity of Activator on the Mechanical Properties of Ground Granulated Blast-Furnace Sla.

[13] Das, S., Saha, P., Jena, S. P., & Panda, P. (2022). Geopolymer concrete: Sustainable green concrete for reduced greenhouse gas emission–A review. Materials Today: Proceedings, 60, 62-71.

[14] Rajmohan, B., Nayaka, R. R., Kumar, K. R., & Kaleemuddin, K. (2022). Mechanical and durability performance evaluation of heat cured low calcium fly ash based sustainable geopolymer concrete. Materials Today: Proceedings, 58, 1337-1343.

[15] Chavda, D. C., Pitroda, J. R., & Vaghela, K. Experimental Study on Geopolymer Concrete Using Waste Ceramic Powder: A Review.

[16] Öz, A., Bayrak, B., Kavaz, E., Kaplan, G., Çelebi, O., Alcan, H. G., & Aydın, A. C. (2022). The radiation shielding and microstructure properties of quartzic and metakaolin based geopolymer concrete. Construction and Building Materials, 342, 127923.

[17] El-Mir, A., El-Hassan, H., El-Dieb, A., & Alsallamin, A. (2022). Development and Optimization of

Geopolymers Made with Desert Dune Sand and Blast Furnace Slag. Sustainability, 14(13), 7845.

[18] Yoo, D. Y., Lee, S. K., You, I., Oh, T., Lee, Y., & Zi, G. (2022). Development of strain-hardening geopolymer mortar based on liquid-crystal display (LCD) glass and blast furnace slag. Construction and Building Materials, 331, 127334.

[19] Kheimi, M., Aziz, I. H., Abdullah, M. M. A. B., Almadani, M., & Abd Razak, R. (2022). Waste Material via Geopolymerization for Heavy-Duty Application: A Review. Materials, 15(9), 3205.

[20] Zeyad, A. M., Magbool, H. M., Tayeh, B. A., de Azevedo, A. R. G., Abutaleb, A., & Hussain, Q. (2022). Production of geopolymer concrete by utilizing volcanic pumice dust. Case Studies in Construction Materials, 16, e00802.

[21] Bhaskar, M. U., & Prashanth, M. (2022). SILICAFUME BASED GEOPOLYMER CONCRETE-DURABILITY PROPERTIES FOR M60 GRADE. NeuroQuantology, 20(6), 5415-5425.

[22] Arunachelam, N., Maheswaran, J., Chellapandian, M., Murali, G., & Vatin, N. I. (2022). Development of High-Strength Geopolymer Concrete Incorporating High-Volume Copper Slag and Micro Silica. Sustainability, 14(13), 7601.

[23] Bellum, R. R., Al Khazaleh, M., Pilla, R. K., Choudhary, S., & Venkatesh, C. (2022). Effect of slag on strength, durability and microstructural characteristics of fly ash-based geopolymer concrete. Journal of Building Pathology and Rehabilitation, 7(1), 1.

[24] Thomas, B. S., Yang, J., Bahurudeen, A., Chinnu, S. N., Abdalla, J. A., Hawileh, R. A., ... & Hamada, H. M. (2022). Geopolymer concrete incorporating recycled aggregates: A comprehensive review. Cleaner Materials, 100056.

[25] Farokhzad, R., Mohammadbeigi, A. (2022). Evaluating Compressive and Tensile Strength and Water Absorption of Geopolymer Mortar Containing Slag (GGBFS) in Comparison with Pozzolan Metakaolin. Journal of Structural and Construction Engineering, 8(11), 292-3.

[26] Shilar, F. A., Ganachari, S. V., Patil, V. B., Khan, T. Y., Almakayeel, N. M., & Alghamdi, S. (2022). Review on the relationship between nano modifications of geopolymer concrete and their structural characteristics. Polymers, 14(7), 1421.

[27] Li, B., Tang, Z., Huo, B., Liu, Z., Cheng, Y., Ding, B., & Zhang, P. (2022). The Early Age Hydration Products and Mechanical Properties of Cement Paste Containing GBFS under Steam Curing Condition. Buildings, 12(10), 1746.

[28] Mansourghanaei, M., Biklaryan, M., & Mardookhpour, A. (2022). Experimental study of the effects of adding silica nanoparticles on the durability of geopolymer concrete. Australian Journal of Civil Engineering, 1-13.

[29] Mansourghanaei, M., Biklaryan, M., & Mardookhpour, A. (2022). Experimental study of properties of green concrete based on geopolymer materials under high temperature. Civil Engineering Infrastructures Journal.

[30] Mansourghanaei, M. (2022). Experimental evaluation of compressive, tensile strength and impact test in blast furnace slag based geopolymer concrete, under high temperature. Journal of Civil Engineering Researchers, 4(2), 12-21.

[31] Mansourghanaei, M., Biklaryan, M., & Mardookhpour, A. (2023). Experimental Study of Modulus of Elasticity, Capillary absorption of water and UPV in Nature-Friendly Concrete Based on Geopolymer Materials. International Journal of Advanced Structural Engine.

[32] Xavier, C. S. B., & Rahim, A. (2022). Nano aluminium oxide geopolymer concrete: An experimental study. Materials Today: Proceedings, 56, 1643-1647.

[33] Han, Q., Zhang, P., Wu, J., Jing, Y., Zhang, D., & Zhang, T. (2022). Comprehensive review of the properties of fly ash-based geopolymer with additive of nano-SiO2. Nanotechnology Reviews, 11(1), 1478-1498.

[34] Jin, Q., Zhang, P., Wu, J., & Sha, D. (2022). Mechanical Properties of Nano-SiO2 Reinforced Geopolymer Concrete under the Coupling Effect of a Wet–Thermal and Chloride Salt Environment. Polymers, 14(11), 2298.

[35] Li, L., Sun, H. X., Zhang, Y., & Yu, B. (2021). Surface cracking and fractal characteristics of bending fractured polypropylene fiber-reinforced geopolymer mortar. *Fractal and Fractional*, 5(4), 142.

[36] Li, L., Tao, J. C., Zhang, Y., Sun, H. X., Yuen, K. V., & You, P. B. (2022). Crack fractal analysis of fractured polyethylene fiber reinforced alkali activated mortar under flexural load. *Construction and Building Materials*, 345, 128428.

[37] Lao, J. C., Xu, L. Y., Huang, B. T., Dai, J. G., & Shah, S. P. (2022). Strain-hardening ultra-high-performance geopolymer concrete (UHPGC): Matrix design and effect of steel fibers. Composites Communications, 30, 101081.

[38] Xu, Z., Wu, J., Zhao, M., Bai, Z., Wang, K., Miao, J., & Tan, Z. (2022). Mechanical and microscopic properties of fiber-reinforced coal gangue-based geopolymer concrete. Nanotechnology Reviews, 11(1), 526-543.

[39] Zeyad, A. M., Hakeem, I. Y., Amin, M., Tayeh, B. A., & Agwa, I. S. (2022). Effect of aggregate and fibre types on ultra-high-performance concrete designed for radiation shielding. Journal of Building Engineering, 58, 104960.

[40] Li, W., Shumuye, E. D., Shiying, T., Wang, Z., & Zerfu, K. (2022). Eco-friendly fibre reinforced geopolymer concrete: A critical review on the microstructure and long-term durability properties. Case Studies in Construction Materials, e00894.

[41] Laxmi, G., & Patil, S. G. (2022). Effect of fiber types, shape, aspect ratio and volume fraction on properties of geopolymer concrete–A review. Materials Today: Proceedings.

[42] Chokkalingam, P., El-Hassan, H., El-Dieb, A., & El-Mir, A. (2022). Development and characterization of ceramic waste powder-slag blended geopolymer concrete designed using Taguchi method. Construction and Building Materials, 349, 128744.

[43] Pilehvar, S., Cao, V. D., Szczotok, A. M., Carmona, M., Valentini, L., Lanzón, M., ... & Kjøniksen, A. L. (2018). Physical and mechanical properties of fly ash and slag geopolymer concrete containing different types of micro-encapsulated phase change materials. *Construction and Building Materials*, *173*, 28-39.

[44] Zhang, F., Li, Y., Zhang, J., Gui, X., Zhu, X., & Zhao, C. (2022). Effects of slag-based cementitious material on the mechanical behavior and heavy metal immobilization of mine tailings based cemented paste backfill. Heliyon, e10695.

[45] Wang, Y., Zhong, H., & Zhang, M. (2022). Experimental study on static and dynamic properties of fly ash-slag based strain hardening geopolymer composites. Cement and Concrete Composites, 129, 104481.

[46] Aisheh, Y. I. A., Atrushi, D. S., Akeed, M. H., Qaidi, S., & Tayeh, B. A. (2022). Influence of polypropylene and steel fibers on the mechanical properties of ultra-high-performance fiber-reinforced geopolymer concrete. Case Studies in Construction Materia.

[47] Abbas, A. G. N., Aziz, F. N. A. A., Abdan, K., Nasir, N. A. M., & Huseien, G. F. (2023). Experimental evaluation and statistical modeling of kenaf fiber-reinforced geopolymer concrete. *Construction and Building Materials*, *367*, 130228.

[48] Ali, S., Sheikh, M. N., & Hadi, M. N. (2023). Splitting-and Direct-Tensile Strengths of Ambient Cured Geopolymer Concrete with Glass Fibers. In *8th International Conference on Advanced Composite Materials in Bridges and Structures* (pp. 109-117). Springer, Cham.

[49] Xie, J., Zhao, J., Wang, J., Fang, C., Yuan, B., & Wu, Y. (2022). Impact behaviour of fly ash and slag-based geopolymeric concrete: The effects of recycled aggregate content, water-binder ratio and curing age. Construction and Building Materials, 331, 127.

[50] Wang, Z., Bai, E., Huang, H., Liu, C., & Wang, T. (2023). Dynamic mechanical properties of carbon fiber reinforced geopolymer concrete at different ages. *Ceramics International*, *49*(1), 834-846.

[51] Ahmed, M. F., Khalil, W. I., & Frayyeh, Q. J. (2022). Effect of Waste Clay Brick on the Modulus of Elasticity, Drying Shrinkage and Microstructure of Metakaolin-Based Geopolymer Concrete. Arabian Journal for Science and Engineering, 1-13.

[52] Kaya, M., Koksal, F., Gencel, O., Munir, M. J., & Kazmi, S. M. S. (2022). Influence of micro Fe2O3 and MgO on the physical and mechanical properties of the zeolite and kaolin based geopolymer mortar. Journal of Building Engineering, 52, 104443.

J-Researchers

Analysis of the behavior of reinforced concrete buildings with and without non-buckling braces under the effect of earthquake loads

Alireza Sheikhnasiri [iD]a*

aPh.D Student, Structural Orientation, Faculty of Islamic Azad University, (Chalous Branch), Mazandaran, Chalous, Iran

Abstract

The moment frame is one of the most widely used seismic resistant systems in the world, due to its high formability and flexibility, this system causes a lot of displacement in the structure and force exceeding the capacity of the structural components. The bracing system is a suitable method to control the lateral displacement of the structure and the seismic improvement of the bending frame. The new type of bracing system that is used in the design of new systems and the improvement of old structures is non-buckling bracing, and in this research, their effect on the performance of 4, 7, and 10-story concrete moment frames under the Northridge, San Salvador, and Tabas earthquake has been investigated. The research method in this research is analytical-applied, which the results of this study showed; In the 4-story structure, the amount of wasted energy under the 3 considered earthquakes is equal to 0%, 0%, and 1% without buckling braces and 39%, 48% and 50% in the case with non-buckling braces and in the 7- story structure, the amount of energy consumed under the mentioned 3 earthquakes is equal to 0%, 0% and 0% without buckling braces and 40%, 45% and 51% in the case with non-buckling braces and also in the 10- story structure, the amount of energy consumed under the above 3 earthquakes is equal to 1%, 0% and 11% without buckling braces and 35%, 42% and 45% in the case with non-buckling braces. So, it was concluded that the performance of the structure in the case with non-buckling braces is better than in the case without non-buckling braces. © 2017 Journals-Researchers. All rights reserved. (DOI:**https//doi.org/10.52547/JCER.5.3.35**)
"Keywords: Seismic performance, reinforced concrete frame, non-buckling bracing, Moment frame."

1. introduction

The moment frame system is one of the most widely used seismic resistant systems in the world, due to its high formability and flexibility, this system causes a lot of displacement in the structure and force exceeding the capacity of the components in the structure, and the failure of structural components and it will lead to non-structure [1]. The brace is a stiffening member of the structure against lateral forces such as wind or earthquake forces. Due to the fast implementation compared to the shear wall, it has become very popular among the public, but their incorrect implementation in the building not only does not cause stability but also causes twisting [2]. One of the important problems that occur in ordinary

* Corresponding author. Tel.: +989904417166; e-mail: Alireza.sa30@gmail.com

braces during an earthquake is the issue of buckling of the compression member. During an earthquake, the length of the brace is gradually increased permanently, and in return, this increase in inelastic length leads to premature buckling of the brace, and in the next cycles, it shows late resistance, and this causes more energy to be absorbed in the non-replaceable members and connections of the frame. bending and also increasing the lateral displacement of the structure. The bracing system is a very suitable method to control the lateral displacement of the structure and seismic improvement of the bending frame. The new type of bracing system that is used in the design of new systems and the improvement of old weak structures is non-buckling bracing, and in this research, its effect on the performance of the concrete moment frame is investigated. The non-buckling brace is one of the lateral load-bearing systems that has been expanding its use in structures in the last two decades. This lateral bracing system has replaced conventional braces (buckling braces) in convergent bracing frames due to its good performance. Compared to conventional braces, non-buckling braces exhibit more stable and symmetrical cyclic performance, resulting in significant energy dissipation capacity. The non-buckling brace consists of a ductile steel core. This steel core is placed inside a rectangular or round cross-section that is filled with concrete or mortar. Concrete or mortar that fills between the round or square steel core will delay the local buckling of the brace. The surface of the steel core is covered with a non-stick material to separate the concrete from the steel section. This non-stick material reduces the friction between steel and concrete as much as possible and reduces the transmission of axial force from the steel core to the concrete and the section of the steel shell. Also, because the Poisson effect causes the expansion of the steel core under pressure, so a small distance is needed between the steel core and the concrete. Also, in the compressive area, normal braces have an unstable hysteresis loop and energy absorption is low, while braces braced against buckling in the compressive area have stable hysteresis loops, and energy absorption in the compressive area is equal to the tensile area. This type of structural system acts like a hysteresis damper.

Parvri and Mazaheri (2010), in an article, investigated the effect of connecting beam length on the stiffness and ductility of divergent braces. Divergent EBF braces are among the lateral load-resistant systems that are used together with simple frames or bending frames to deal with the forces caused by earthquakes. Due to the compatibility of such braces with architectural conditions, their use in ordinary buildings is very common. The main advantage of divergent braces compared to convergent braces is their proper plasticity along with their hardness. For this reason, the use of this system in tall buildings where it is not possible to use converging braces is increasing day by day [3].

Jae-Do Kang, and Hiroshi Tagawa (2013), investigated the " Seismic response of steel structures with seesaw systems using viscoelastic dampers ". In his research, he evaluated a new vibration control system based on the seesaw mechanism using BRB. This mechanism can increase the ductility of the brace according to the configuration of the damper system. Seismic response analysis for steel bending frames was done with the proposed control system. The results of displacement periodic time showed that the proposed system can effectively reduce the seismic response of the frame [4].

Shakri et al. (2012) conducted a seismic evaluation of wind-braced structures with CFR columns equipped with viscous dampers. He stated in his research. The amount of damping in normal structures is very low, and therefore these buildings displace a lot under the influence of strong dynamic forces such as earthquakes by passing through the elastic range. The results showed that due to the many advantages of structures with CFT columns and their suitable seismic performance in both areas of hardness and resistance, their seismic behavior is very useful for a seismically prone country like Iran [5].

Asgar (2012), investigated the effects of converging bracing arrangement in the seismic evaluation of steel frames. In this research, three important seismic parameters, which are regulated in most of the seismic regulations, were examined as follows: 1- The maximum global displacement of the roof 2- The maximum relative displacement angle of the floor 3- The maximum local moment with Examining the mentioned indicators in each of the studied frames, the appropriate level is suggested to change the bracing type [6].

Black et al. (2014), review the Design of Seismically Resistant Tree-Branching Steel Frames Using Theory and Design Guides for Eccentrically Braced Frames. This article describes how the theories, protocols, and legal requirements of eccentrically braced frames (EBFs) were applied to the 2009 International Building Code (IBC) and the 2010 California Building Code (CBC) for prestressing steel frames. provide the earthquake and allow the construction of these incompatible geometries [7].

Azad, S. K., & Topkaya (2016), A review of research on steel eccentrically braced frames. The findings of numerical investigations on the seismic performance of EBFs are discussed to provide insight into the appropriate response factors used in the design of these systems. In addition, specific topics and applications of EBFs such as replaceable links are provided. The impact of the research findings on the design of EBFs systems considering AISC seismic regulations for steel structure buildings has been proven [8].

Chang-Hwan Lee et al. (2016); In his research, he addressed the numerical and experimental analysis of the combined behavior of shear-type friction damper and non-uniform strip damper for multi-level seismic protection. The obtained results showed that for metal frame structures of about 8 floors and less consisting of CBF and EBF bracing if the ratio of the number of EBF panels to CBF in each main direction is greater than or equal to three and ≥ 0.3, it can be the coefficient of the behavior of the EBF bracing system was used in the design of structures. By examining the proposed MBF bracing system, it was observed that for 4, 6, and 8-story models, the behavior coefficient of these structures with increasing height tends to the behavior coefficient of the EBF bracing system with medium plasticity, i.e., 7. One of the other advantages of this system is passing through a critical earthquake without destroying the roof beams of the MBF beam floors. The structure returns to its original state. In addition to these advantages, MBF has the possibility of opening installation and has better compatibility with architectural designs [9].

2. Methodology

In this research, a concrete moment frame system with and without non-buckling braces is investigated

using the finite element method and using SAP 2000 software. Assuming that the structure is loaded in the form of the load-bearing width of the opening, and also based on the steel and concrete regulations of Iran, the design of the concrete structure is done. In the following, according to the regulations of 2800 4th edition and ASCE07-10, applied earthquakes are scaled concerning the mentioned structure. Then the cyclic curve of force displacement, energy consumption, and damping are investigated and drawn and compared for both systems.

Based on the present study, using the available resources and related tools, the following goals have been considered:

1- Comparison of the base shear stress applied to the structure in the concrete frame compared to the non-buckling brace

2- Calculation of the maximum displacement of the structure for the concrete frame system with and without buckling braces

3- Investigation of energy consumption and absorbed energy in the concrete frame system with the non-buckling brace

4- Investigating the behavior of force-displacement of non-buckling brace used due to different earthquakes

Buckling-resistant bracing frames (BRB) are a special type of convergent bracing frame in which the buckling of the bracing is prevented by special measures. Figure (1) shows a comparison between the behavior of a non-buckling brace and a normal convergent brace in a loading cycle.
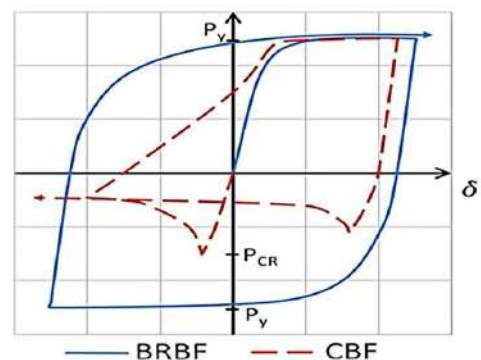

Fig. 1. Behavioral comparison between normal braces and non-buckling braces [10]

In this study, the buildings are the residential type with medium importance and in the area with relatively high risk. The land used is type II and the

building is of moment frame concrete type. The floors have a rigid diaphragm, and also in the design of the models, the topics of the National Building Regulations, ASCE07-10, Publication 360, and the 2800 Regulations (4th Edition) have been used.

3. Results and discussion

According to the hysteresis diagram of the 4-story structure, it was observed that the bracing entered the non-linear range in the Tabas earthquake and has a larger area under the diagram. The hysteresis curve of the brace in all earthquakes has the same dissipated force but different displacement. The non-buckling brace behaves in the same way as tension in compression, so its hysteresis curve has positive and negative areas. The maximum longitudinal displacement of the brace was equal to 10 cm. Figure (2) shows a comparison between three considered earthquakes for a 4-story structure.
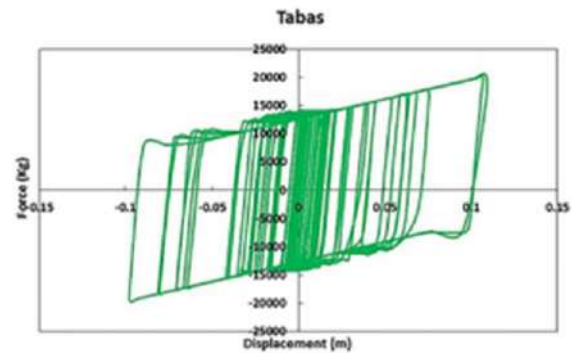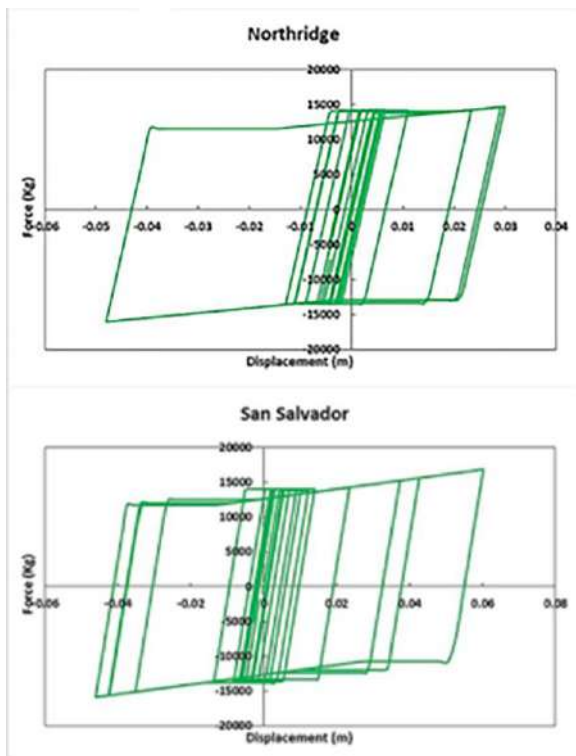
Fig. 2. Hysteresis behavior of non-buckling bracing in a 4-story building under three earthquakes: Northridge, San Salvador, and Tabas

According to the hysteresis diagram of the 7-story structure, it was observed that the bracing entered the non-linear range in the Tabas earthquake and the area under the diagram is larger. The hysteresis curve of the brace in all earthquakes has the same dissipated force but different displacement. The non-buckling brace behaves in the same way as tension in compression, so its hysteresis curve has positive and negative areas. The maximum longitudinal displacement of the brace was 10.5 cm. Figure (3) shows a comparison between three considered earthquakes for a 7-story structure.
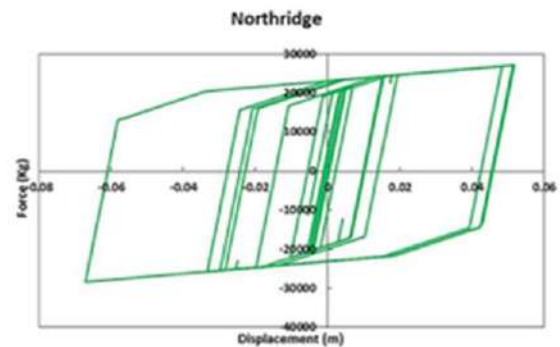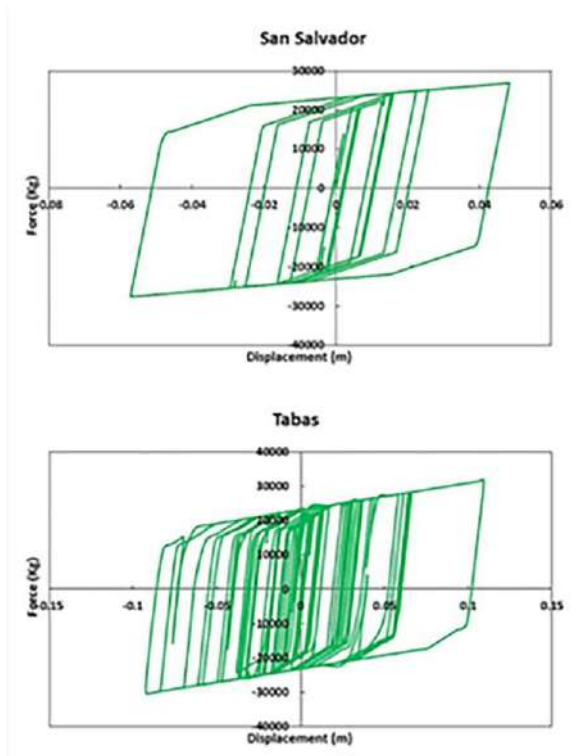
Fig. 3. Hysteresis behavior of non-buckling bracing in a 7-story building under three earthquakes: Northridge, San Salvador, and Tabas

According to the hysteresis diagram of the 10-story structure, it was observed that the bracing entered the non-linear range in the Tabas earthquake and has a larger area under the diagram. The hysteresis curve of the brace in all earthquakes has the same dissipated force but different displacement. The non-buckling brace behaves in the same way as tension in compression, so its hysteresis curve has positive and negative areas. The maximum longitudinal displacement of the brace was equal to 10 cm. Figure (4) shows a comparison between three considered earthquakes for a 10-story structure.
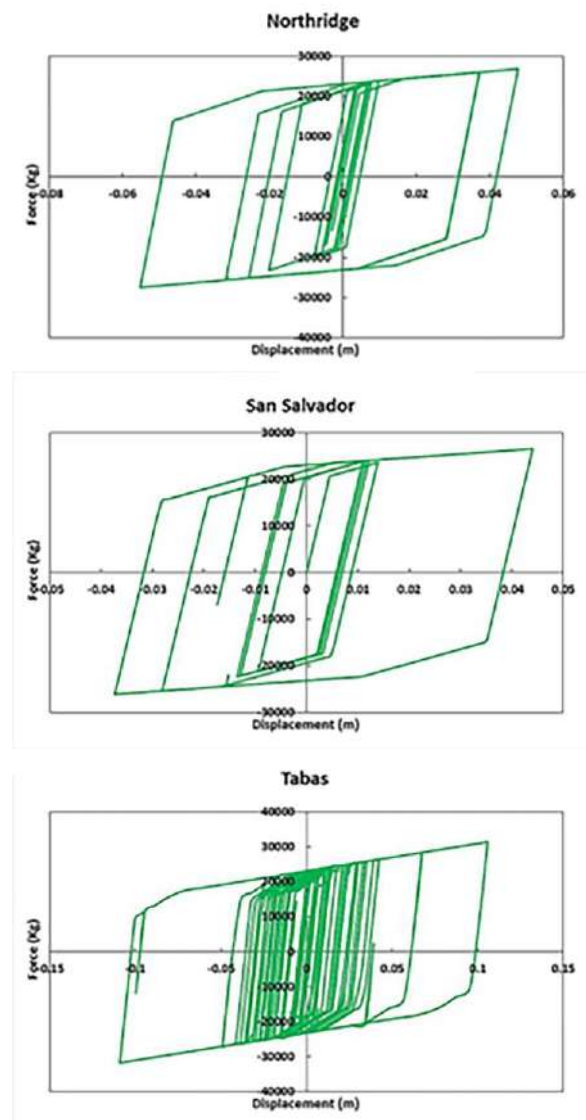
Fig. 4. Hysteresis behavior of non-buckling bracing in a 7-story building under three earthquakes: Northridge, San Salvador, and Tabas

4. Conclusions

In the present study, the general results of the analysis of 4, 7, and 10-story buildings under renovation with passive non-buckling bracing systems have been obtained as follows.

- In the 4-story structure, the amount of energy consumed under the 3 earthquakes of Tabas,

Northridge, and San Salvador in the case without non-buckling braces is equal to 0%, 0%, and 1% and in the case with non-buckling braces is equal to 39%, 48% and it is 50%.

- In the 7-story structure, the amount of energy consumed under the 3 earthquakes of Tabas, Northridge, and San Salvador in the case without buckling brace is equal to 0%, 0%, and 0% and in the case with buckling brace is equal to 40%, 45% and 51 % is

- In a 10-story structure, the amount of energy consumed under the 3 earthquakes of Tabas, Northridge, and San Salvador in the case without buckling braces equals 1.1%, 0%, and 11%, and in the case with braces equal to 35%, 42% and it is 45%.

- In each earthquake, the amount of energy consumption is different, but in general, the average energy consumption in 4, 7, and 10-story structures was higher, respectively, and this average decreased with the increase in height.

- as the results say; The performance of the structure in the case with non-buckling bracing is better than in the case without non-buckling bracing. High consumption of energy in the structure reduces the effects of earthquakes on the structure and also reduces seismic damage in non-structural elements and joinery.

- The displacements of the structure by using non-buckling braces have been significantly reduced and this reduction of displacements has caused the control of the drift of the structure.

- In examining the displacement of the 4, 7, and 10-story structures, the maximum displacement occurred in the structure under the Tabas earthquake, which is 100, 185, and 240 cm without non-buckling braces and 63, 98, and 167 cm in the case with non-buckling braces. The fact that the structure has had a lot of displacement should be investigated in the environmental conditions of the structure, whether the structure can have this amount of displacement or is there a limit.

- In the examination of foundation shear of 4, 7, and 10-story structures, the maximum amount of foundation shear occurred in the structure under the Tabas earthquake, which is 1,400, 2,000, and 1,800 tons without non-buckling braces, and

1,000, 1,300 And 1700 tons with braces. The shearing of the foundations of the structure by using non-buckling braces has been significantly reduced, and this reduction of shearing of the foundation has led to the control of the structure, and therefore, the use of light sections and low earthquake force on the structure makes the design more economical.

References

[1] Hale, T., Pall, R., (2000) "Seismic Upgrade of the Freeport Water Reservoir, Sacramento, California", Proceedings, Twelfth World Conference on Earthquake Engineering, Auckland, NZ. Paper No. 269

[2] Vail, C., Hubbell. O'Connor, B., King, J., Pall, A, (2004) "Seismic Upgrade of Boeing Commercial Airplane Factory at Everett, WA", Proceedings, Thirteenth World Conference on Earthquake Engineering, Vancouver, Paper No.3207.

[3] Parvri, Ali; Mazaheri, Hamid. (2018). Investigating the effect of connecting beam length on stiffness and ductility of divergent braces, 6th National Congress of Civil Engineering

[4] Jae-Do Kang, Hiroshi Tagawa. (2013)." Seismic response of steel structures with seesaw systems using viscoelastic dampers". Authors. Volume 42, Issue 5. 25 April 2013.Pages 779–794.

[5] Shakri, Seyed Hashem; Waqfi, Mohammad; Nagaristan, Zari. (2012). Seismic evaluation of wind-braced structures with cfr columns equipped with mirage-viscous. 7th National Congress of Civil Engineering. Article ID (COI): NCCE07_0388.

[6] Asgar, Mustafa; (2012). Effects of converging bracing arrangement in the seismic evaluation of steel frames. Master's thesis. Ministry of Science, Research and Technology - Aba non-profit and non-governmental higher education institute - Faculty of Civil Engineering.

[7] Black, R. G., & Astaneh-Asl, A. (2014). Design of Seismically Resistant Tree-Branching Steel Frames Using Theory and Design Guides for Eccentrically Braced Frames. World Academy of Science, Engineering, and Technology, International Journal of Civil, Environmental, Structural, Construction, and Architectural Engineering, 8(2), 206-213.

[8] Azad, S. K., & Topkaya, C. (2016). A review of research on steel eccentrically braced frames. Journal of Constructional Steel Research, 128, 53-73.

[9] Chang-Hwan Lee, Jinkyu Kim, Do-Hyun Kim, Jaeho Ryu, Young K. Ju. (2016)." Numerical and experimental analysis of combined behavior of

shear-type friction damper and non-uniform strip damper for multi-level seismic protection". Volume 114, 1 May 2016, Pages 75–92.

[10] Naqipour, Morteza; Bahrami, Seyyed Reza Salim, Nemati, Marzieh, (2014), The role of elements with ductile behavior in the seismic performance of frames with convergent bracing, Imran Modares scientific-research journal, 15th volume, number 1.

Investigation and comparison of numerical methods in predicting the behavior of rebar in reinforced concrete hollow slab (from start to crack) in Abaqus finite element software

Pouria Niknafs [iD][a*]

[a]Ms.c student, Department of Civil Engineering, Centeral Tehran Branch, Islamic Azad University, Tehran, Iran

Abstract

Nowadays, the use of reinforced concrete hollow slab system in building structures is widely accepted due to the provision of control criteria, the ability to be used in large openings and flexibility in architectural designs, and it is more responsive in terms of economic efficiency and time management. has it. The use of reinforced concrete hollow slabs is one of the effective methods in styling and reducing the dead load and consequently the earthquake load, and as a result achieving sections with smaller dimensions. The aim of the current research is to study the post-cracking behavior of reinforced concrete hollow slabs under Common loading situations and analyzed using the finite element method. Also, by using the obtained results and comparing them with the behavior of laboratory samples, it is intended to determine the optimal numerical model for predicting the behavior of reinforced concrete hollow slab, and to measure the accuracy of common design relationships. Modeling of hollow concrete slab sample in this study has been done using ABAQUS software, and the results of this study showed; The load coincident with the first crack in the CDP method was obtained for 10.18, 15.2, 34.20, and 44 for the concentrated joint, concentrated grip, wide joint, and wide grip modes, respectively. © 2017 Journals-Researchers. All rights reserved. (DOI:**https//doi.org/10.52547/JCER.5.3.42**)

1. Introduction

The most important challenge for engineers in analyzing the behavior of reinforced concrete members is to predict how cracks form and spread and its effect on various components such as hardness, load, deformations, durability and serviceability of these members. Slabs are one of the important components of structures that are responsible for carrying most of the loads on the structure; There are various methods for predicting the behavior of common and solid signs, the most important of which are theories based on fault lines, which are widely used

_____
* Corresponding author. Tel.: +98-912-312-3545; e-mail: pourianiknafs@gmail.com.

by designers. Regarding hollow slabs, despite their increasing use, it can be said that due to the variety of geometry and characteristics of holes or internal cavities of these slabs, there are many fields for research, which is especially important in The field of predicting the

occurrence and spread of cracks and its impact on the general behavior of the member is doubly important, especially that the various theories and relationships proposed by researchers in the field of crack analysis also have a lot of variety and according to the young The relative nature of this branch of science, the evaluation of their efficiency in hollow signs also requires extensive experimental and theoretical investigations.

The first research in the field of perforated slabs was done by Clark and Oduyemi [1], who specified in an article that the maximum amount of tensile hardening was created. In perforated slabs with tubular holes, it is subject to strain and cracked network of concrete in the natural axes of the section. In one of the conducted researches, it is emphasized that in general, the presence of longitudinal tubular holes reduces the rate of crack growth and also the cross-sectional strength of the slab, depending on the size of the holes and the dimensions of the slab[2],[3]. In another article, Al-Awazi and Al-Asadi [4], [5] point out that Turkish. In perforated slabs, they expand at a lower speed than in normal slabs.

Among others, the research conducted on the performance of hollow slabs after cracking was done by Schwetz [6], which shows the effect of cracking on the curvature of hollow slabs, and in which a numerical modeling is a solution for optimization. and provides reinforcement of hollow slabs.

In another research, Schwetz deals with the numerical and laboratory investigation of a hollow slab, and the laboratory model shows a behavior similar to the numerical sample in its linear behavior [6].

The use of hollow slabs is one of the effective methods in styling and reducing the dead load and consequently the earthquake load, and as a result achieving sections with smaller dimensions. On the other hand, due to the brittleness and brittle nature of concrete slabs, the presence of initial pressure on the concrete piece causes the concrete to stretch and crack later as a result of loading. Therefore, the comparative

study of numerical methods for predicting the behavior after cracking of reinforced concrete hollow slabs is very important, which is considered in this study. Therefore, according to the above interpretations; In this research, an attempt has been made to analyze and compare the numerical methods of predicting the behavior of reinforced concrete hollow slabs after cracking.

2. Research method and modeling

This study is analytical-applied as well as laboratory, and the method of analysis in this research is done using ABAQUS finite element software and ETABS software. After studying the background of the work and examining the relevant behavioral models and theories in the field of crack analysis in reinforced concrete sections, by selecting the results of a number of valid laboratory studies in the field of hollow slabs, the relevant samples were modeled and analyzed. is placed and the accuracy and efficiency of the relevant models are checked and the most suitable behavioral models are selected.

Then, by using the relations proposed by the regulations and authoritative references in the field of designing hollow slabs, the accuracy of the application of these relations was measured and the necessary solutions for the optimal design of hollow slabs according to the type of loading, support conditions and geometrical specifications. Holes will be provided

2.1. Concentrated load with simple support:

The compressive behavior of concrete is defined based on the modified Hagenstad model for both investigated methods. Tensile behavior of concrete based on Wahalatantri model is used for CDP method. In the initial model, the CDP method is used to check the hollow slab. In the above method, the damage criterion is used to reduce the strength of concrete after cracking. The dynamic and static solver can be used to solve the numerical models made by the above method, in this study, the dynamic solver was used due to the convergence problems of the static solver. The displacement force diagram of the model is compared

with the experimental sample, which is shown in the figure below.
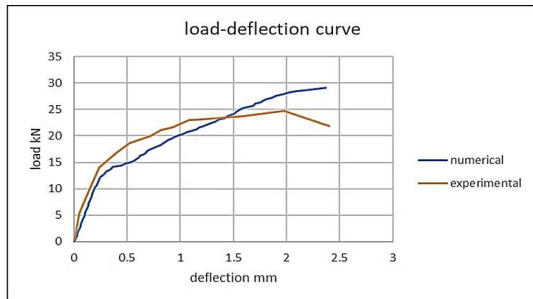

Diagram 1- Comparison of the displacement force diagram of the model with the laboratory sample in the case of a concentrated load with a simple support(Source: Researcher)

The tensile damage criterion has been used to investigate the crack growth process and as can be seen in Figure (1), the first cracking is shown at a load of 10.18 kN. Also, the criterion of the main maximum plastic strain has been used to check the crack initiation location, which is shown in Figure (2).
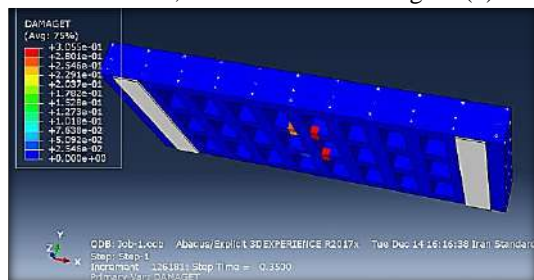
Figure 1- The picture of the investigation of the crack growth process using the tensile damage criterion in the case of a concentrated load with a simple support (Source: Researcher)

The cracks created in the hollow slab after applying the loading mentioned in the article, based on the criteria of tensile damage and maximum main strain, are shown in Figures (3) and (4).

Figure (5) display of stresses along the vertical axis (shear stress); The colors indicates that the stress is almost uniformly distributed on the surface of the slab.

Therefore, according to figure (6), the schematic representation of the stresses in the longitudinal direction of the rebars in the CDP method indicates that the rebars have reached yield in the central part of the slab.
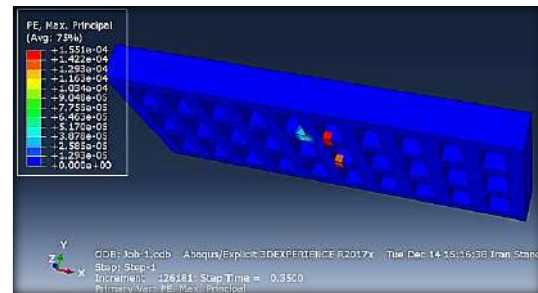
Figure 2- The picture of the location of the crack initiation using the criterion of the main maximum plastic strain in the case of concentrated load with a simple support(Source: Researcher)
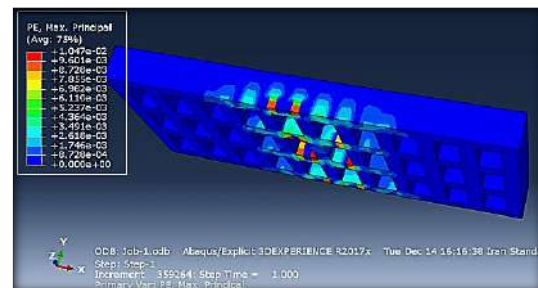
Figure 3- The cracks created in the hollow slab after applying the load based on the tensile damage criterion in the CDP method(Source: Researcher)
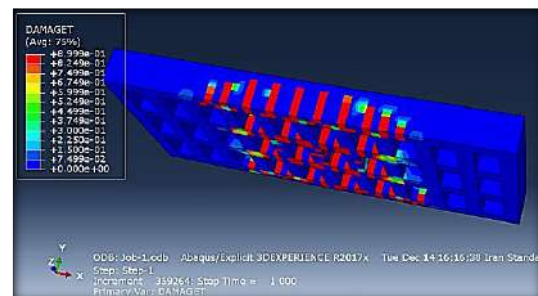
Figure 4- The cracks created in the hollow slab after applying loading based on the maximum main strain criterion in the CDP method

In addition to the aforementioned method; Another method called SCC has been used to model concrete and investigate the propagation of cracking in concrete. In the above method, only the static solver can be used to solve the numerical model, which leads to convergence problems of the solver. The compressive behavior of concrete can be defined in a non-linear way as in the previous method. But in this

method, it will not be possible to reduce the hardness of loading after cracking. For this reason, the damage criterion can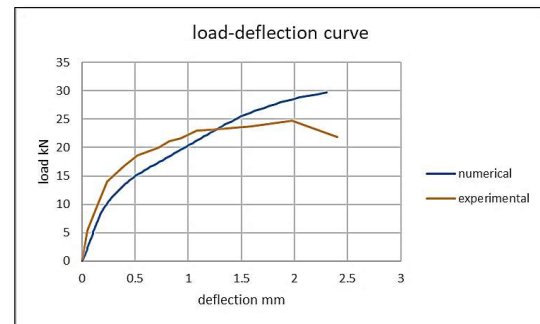not be defined and checked in the above model. The force-displacement diagram of the numerical model made by the above method is compared with the force-displacement diagram of the experimental model in diagram (2), which is in good agreement and shows no difference worth mentioning in the calculations. The figure below compares the load-displacement diagram of the laboratory mode and the numerical mode of smeared cracking.
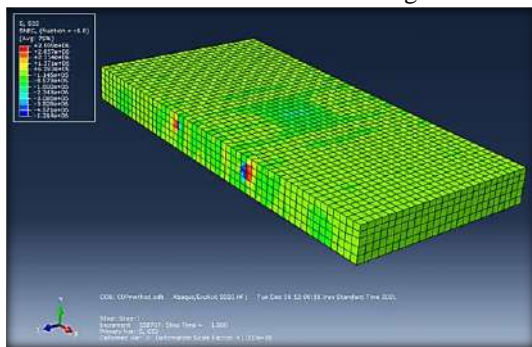
Figure 5- Image of stresses along the vertical axis (shear stress) in the case of concentrated load with simple support
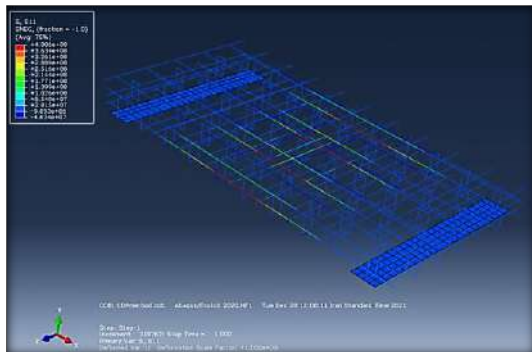
Figure 6- Schematic representation of the stresses in the longitudinal direction of the rebars in the CDP method in the case of concentrated load with simple support

Also, the main maximum plastic strain occurred during the first crack at a load of 6.58 kN, which can be seen in Figure (7).

Diagram 2- The force-displacement diagram of the numerical model made by the scc method with the force-displacement diagram of the experimental model in the case of concentrated load with a simple support
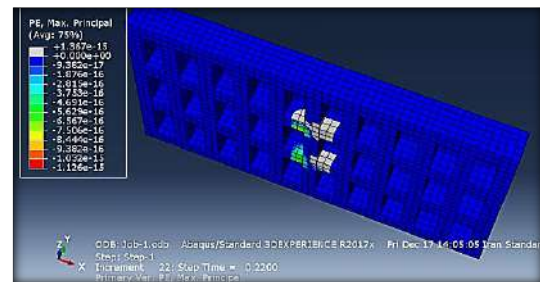
Figure 7 - The image of the main maximum plastic strain during the first crack in the scc method in the case of concentrated load with simple support
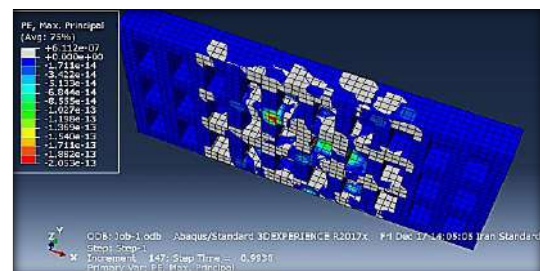
Figure 8 - The image of the main maximum strain after applying loading in the scc method

The main maximum strain after applying the load, which indicates the cracked areas in the concrete, is shown in Figure (8).

Therefore, based on the analysis done, finally, the load-displacement comparison chart obtained from the two CDP and Smeared Cracking methods is in the form of chart (3).
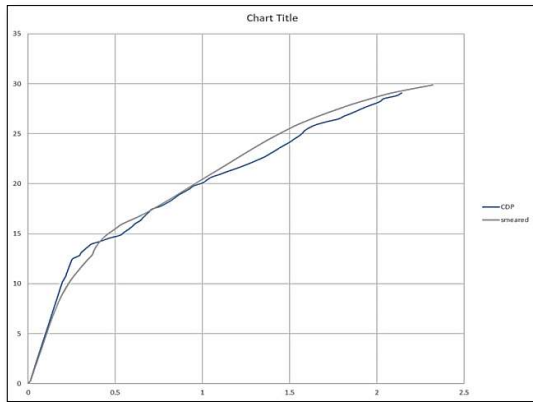
Diagram 3- Load-displacement comparison diagram resulting from CDP and Smeared Cracking methods in the case of concentrated load with simple support
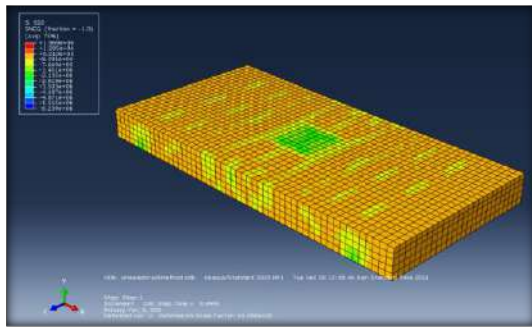
Figure 9- Display of stresses along the vertical axis for semi-concentrated load and simple support in Smeared Cracking method
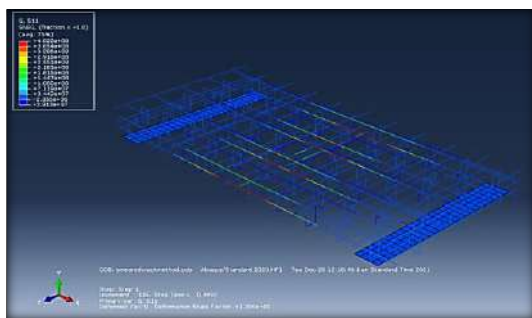
Figure 10- Showing the stresses in the longitudinal direction of the rebars in the smeared cracking method

As can be seen in the diagram (3); In the case of concentrated load with simple support, both methods agree well up to a loading of 7 kN, but after that the

Smeared Cracking method tends to show an almost trilinear mode. Therefore, in general, the two methods have a relatively similar performance in the case of simple support with semi-concentrated loading, and the slope of the displacement load diagram is almost close to each other.

Figure (9) shows the stresses along the vertical axis for the semi-concentrated load and simple support in the Smeared Cracking method, which, like the CDP method, is approximately uniform according to the coloring of the stress distribution, and due to the shape of the loading, the concentration of shear stress in the loading area is less.

Figure (10) shows the stresses in the longitudinal direction of the rebars in the smeared cracking method and as in the CDP method, they have reached yield in the center of the slab.

In general, in the concentrated loading model with a simple support, the behavior of the CDP method in the linear region has a greater slope than the spreading crack mode. Both methods have good compliance, but due to the definition of failure in the plastic rupture method, the accuracy of the results is closer to the laboratory sample.

So far, a load equal to 30 KN according to the laboratory sample was applied to the hollow slab sample on an area of 0.13 x 0.13 square meters and the results were analyzed. In the next part, the sample model made for two broad and semi-concentrated loading conditions (same as the laboratory load) and two simple and fixed support conditions and their combination are examined.

2.2. Wide load with simple support:

For the extended load case, the extended force equal to 60 KN was applied widely to the supports on both sides, and the load-displacement diagram was as follows.

According to the diagram (4) for the case of extended load with simple support, the slope of the linear part of the CDP method diagram is higher and this linear function continues up to the load of 33.6 kilonewtons. But in the Smeared Cracking method, the performance is still almost three-line, and the slope of the initial part is gentler and has a linear performance up to the load of 19.2 kN. Also, the load equivalent to the first crack in the CDP method was equal to 34.2

kilonewtons and for the smeared cracking method it was equal to 42.19 kilonewtons and the cracks were shown in Figure (11).
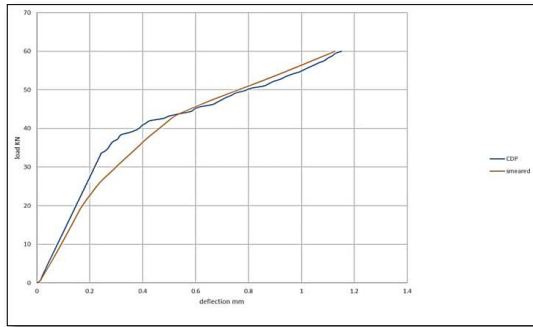

Diagram 4- Comparison diagram of load-displacement resulting from two CDP and Smeared Cracking methods in the case of extended load with simple support
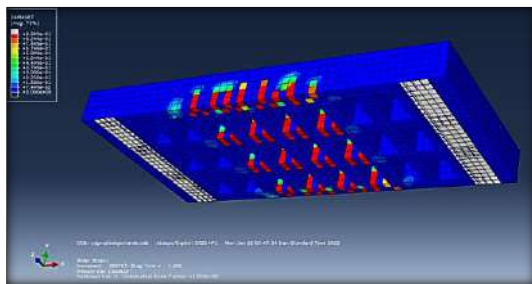

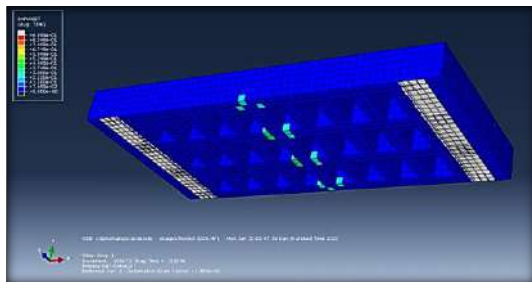Figure 11- CDP cracking (tensile damage t model) in the case of extended load with simple support

Figure 12- The first crack of CDP (tensile damage t) in the case of extended load with simple support

The cracks created in the hollow slab after applying the load, based on the criteria of tensile damage and maximum principal strain, are shown in the following figure 11 and 12.
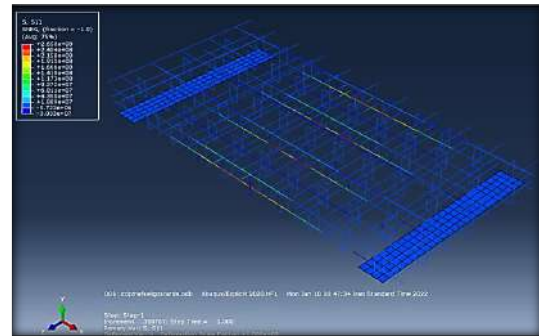
Figure 13 - Showing the stresses in the longitudinal direction of the rebars in the CDP method of simple support extended load
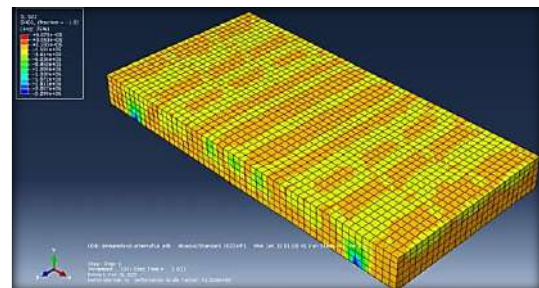
Figure 14 - Display of stresses along the vertical axis for the case of extended load and simple support in the Smeared Cracking method

As can be seen in the picture (12); The first cracks are formed in the middle part of the slab and are of the tensile type that occurred in the extended load state with a simple support.

As can be seen in the picture (12); The first cracks are formed in the middle part of the slab and are of the tensile type that occurred in the extended load state with a simple support.

Figure (14) shows the stresses along the vertical axis for the case of wide load and simple support in the Smeared Cracking method, and according to the figure above, the distribution of stresses is approximately uniform.

Figure (15) showing the stresses in the longitudinal direction of the rebars in the Smeared Cracking method of the extended load with a simple support, which have yielded in the middle part of the slab. In general, in the case of extensive loading with simple support in both methods, the cracks start and expand in the middle part of the slab opening. According to the definition of tensile failure in the CDP method,

there is more accuracy in the display and prediction of cracks, while the prediction of cracks in the propagation crack method is less accurate and mostly has a uniform behavior. In this case, the plastic rupture method shows more hardness and its linear performance continues up to higher loading values.
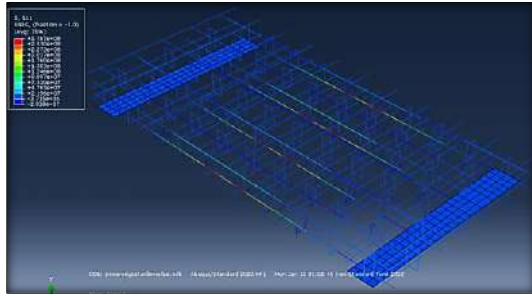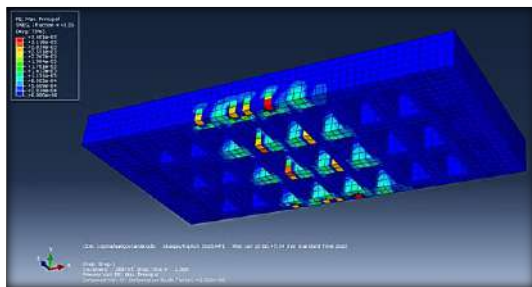

Figure 15 - Showing the stresses in the longitudinal direction of the rebars in the Smeared Cracking method of the extended load with a simple support

Figure 16- The maximum principal strains for the case with a simple support

As can be seen in Figure (17); The crack initiation location based on the maximum principal strain is shown in the figure above, which is consistent with the failure model

The main maximum strain after applying the load, which shows the cracked areas in the concrete in the smeared cracking method, is shown in Figure (18).

The criterion of the main maximum plastic strain has also been used to check the crack initiation location in the Smeared Cracking method. As can be seen in the figure (19), the initial cracks are some distance from the center of the slab, unlike the CDP method.
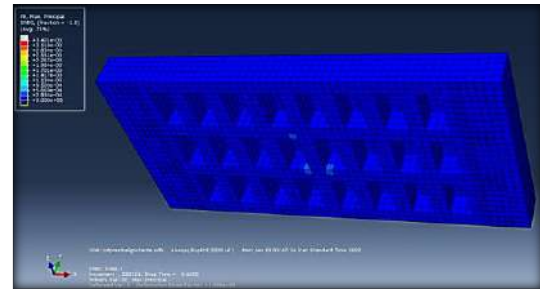
Figure 17 - The image of the crack initiation location based on the maximum main strain in the extended load mode with simple support
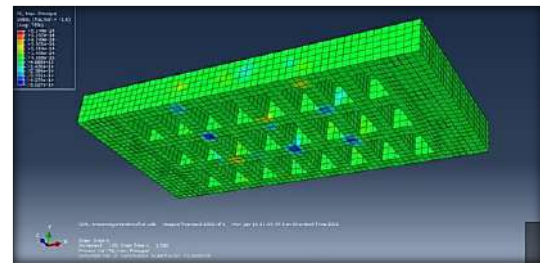

Figure 18 - The image of the main maximum strain after applying the load in the smeared cracking method and in the extended load mode with a simple support
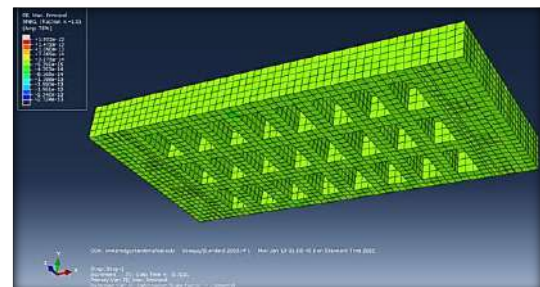

Figure 19 - The standard image of the main maximum plastic strain to check the crack initiation location in the smeared cracking method and in the extended load mode with a simple support

Figure (20) showing the stresses along the vertical (shear) axis for the case of wide load and simple support in the CDP method, which has a uniform value according to the color scheme.

The figure (21) shows the stresses in the longitudinal direction of the rebars in the CDP method.

The figure (22) shows the stresses along the vertical axis for the case of extended load and supporting

support in the smeared cracking method, and according to the image, the stress distribution is almost uniform.
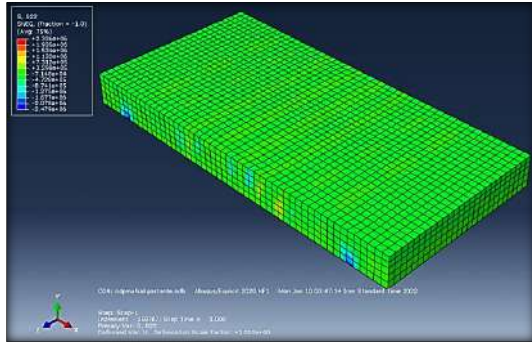

Figure 20 - Showing the stresses along the vertical (shear) axis for the extended load and simple support in the CDP method
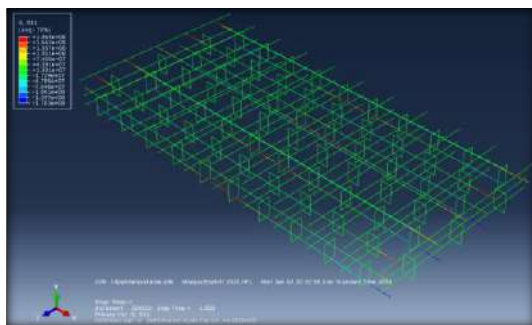

Figure 21- Showing the stresses in the longitudinal direction of the rebars in the CDP method of the extended load of the girder support and the rebars
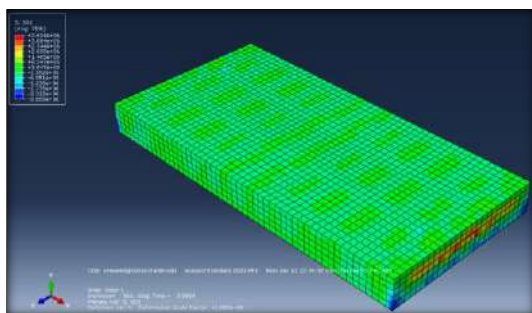

Figure 22 - Display of stresses along the vertical axis for the extended load and supporting support in the smeared cracking method

In general, in the case of extended load with girder support, the cracks start from the support area, with the difference that in the CDP method, the crack occurs in

the upper web and in the Smeared Cracking method, the crack occurs in the lower slab. In this case, the slab shows a relatively harder performance in loading in the CDP method.
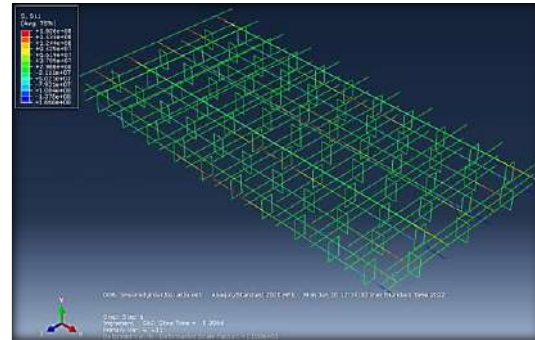

Figure 23- Showing the stresses in the longitudinal direction of the rebars in the smeared cracking method of the extended load of the girder support

3. Conclusion

Based on the analysis done in this study, the results obtained are as follows:

1) Schematic representation of stresses in the longitudinal direction of the rebars in the CDP method indicates that the rebars have reached yield in the central part of the slab.

2) The main maximum plastic strain occurred during the first crack at a load of 6.58 kN.

3) In the case of concentrated load with simple support, both methods are in good agreement with each other up to a loading of 7 kN, but after that the Smeared Cracking method tends to exhibit an almost trilinear mode.

4) Two methods in the case of simple support with semi-concentrated loading have relatively similar performance and the slope of the displacement load diagram is almost close to each other.

5) Showing the stresses along the vertical axis for the semi-concentrated load and simple support in the Smeared Cracking method, which, like the CDP method, is approximately uniform due to the coloring of the stress distribution, and due to the shape of the loading, the concentration of the shear stress in the loading area is less. be

6) Displaying the stresses in the longitudinal direction of the rebars in the smeared cracking method

and as in the CDP method, they have reached yield in the center of the slab.

7)   In general, in the concentrated loading model with a simple support, the behavior of

8)   the CDP method in the linear region has a greater slope than the spreading crack mode. Both methods have good compliance, but due to the definition of failure in the plastic rupture method, the accuracy of the results is closer to the laboratory sample.

References

[1] Adel A. AI- Azzwi and Abbas J., AL-Asdi. 2017. Nonlinear behavior of one way reinforced concrete hollow block slabs.

ARPN Journal of Engineering and Applied Sciences. ISSN 1819-6608

[2] Adel A. Al-Azzawi and Sadeq Aziz Abed. 2016. Numerical analysis of reinforced concrete hollow-core slabs. ARPN Journal of Engineering and Applied Sciences. ISSN 1819-6608

[3] HELÉN BROO.2008. Shear and Torsion in Concrete Structures Non-Linear Finite Element Analysis in Design and Assessment. Chalmers University Of Technology. Göteborg, Sweden.

[4] L. A. Clarck, T. 0. S. Oduyemi. 1987. Tension stiffeningin longitudinal sections of circular voided concrete slabs. Proc. lnstn cio. 861-874

[5] P. F. Schwetz, F. P. S. L. Gastal, L. C. P. Silva. 2009. Numerical and experimental study of a real scale waffle slab. Ibracon structures and materials journal. ISSN 1983-4195

[6] P. F. Schwetz, B. R. B.Recalde, F. P. S. L. Gastal, V. R. D'A Bessa. 2015. Numerical analysis of waffle slabs in flexure considering the effects of concrete cracking. Ibracon structures and materials journal. ISSN 1983-4195.

Modeling and characterization of fiber-reinforced (FRP) plastic honeycomb sandwich panels for bridge deck

Ali nazemideylami [ID][a,*]

ᵃ Ms.c, Department of Civil Engineering, Takestan Branch, Islamic Azad University, Qazvin, Iran

Abstract

Several factors and reasons, including correcting errors in bridge design and construction, preventing damage caused by natural and environmental factors, forces caused by earthquakes, or strengthening the bridge structure to withstand more loads, increase the need to strengthen the bridge. Reinforcement is usually applied to a specific element in the bridge, such as the foundation, column, beam head and deck, each of which may be reinforced. Also, from the economic point of view, retrofitting of bridges is generally preferred compared to the replacement and renovation option. Bridges play an important role in rescue operations after an earthquake. It is necessary that these structures have a higher level of protection against seismic attacks. The earthquake identified the weak points of the structure. Bridges are very vulnerable to these attacks due to their low degree of uncertainty. Seismic displacements based on the principles of elastic design are much less than what the structure experiences in a real earthquake. One of the consequences is the falling of the decks due to the loss of the support surface. The decision to strengthen the bridge was made when many bending and shear cracks were created on the king beams of the bridge. The use of FRP profiles can significantly prevent losses caused by corrosion and is a good alternative to traditional methods of strengthening the structure. In this article, the design for the deck of a sandwich panel bridge reinforced with FRP fibers is presented. © 2017 Journals-Researchers. All rights reserved. (DOI:**https//doi.org/10.52547/JCER.5.3.51**)

1. Introduction

At present, two major types of FRP deck are currently used in engineering works; Sandwich structure and pultruded structure. Sandwich structures consist of strong, high-stiffness top sheets that can withstand bending loads and have very low density.

The core of shear strength is placed between the top sheet and the bottom sheet, which determine the performance of the deck composite. The top sheets are usually made of matrial E-glass or a top of polyester or vinyl ester. The core materials are rigid foam or FRP materials in the form of thin-walled cells shown in Figure 1. Cellular materials are the most important

_____

* Corresponding author. Tel.: +98-911-243-5320; e-mail: Nazemideylami@gmail.com.

materials for structural weight-sensitive applications. Figure 2 shows the sections of the FRP bridge deck.
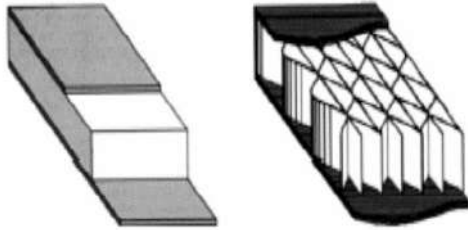

Fig. 1. Examples of types of bridge structures with FRP decks [1]
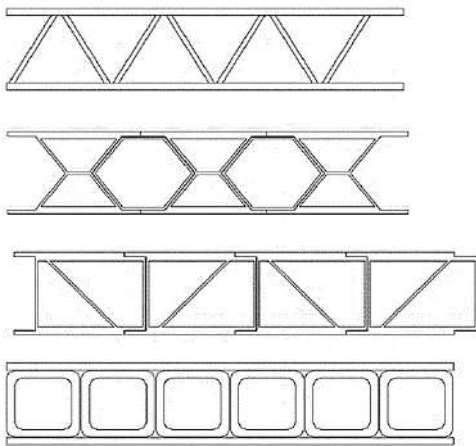

Fig. 2. Types of FRP bridge deck sections. [1]

The failure mechanism in different panels is different according to their load transfer type. For example, the transfer of load in a triangular panel is two-way, and in honeycomb panels, the load is transferred to the four sides of the transfer edge and then transferred to the support. In the following, in this report, the types of panel ruptures (abrasion rupture, shear rupture, bending strain, etc.) are explained and how the load is transferred in all types of panels according to the inner core. An example of failure is presented in Figure 3 related to the triangular panel.

The ability to transfer the load of the honeycomb core of the panel is not completely clear. Therefore, to determine the effective width of the design, it is necessary to consider some assumptions. For this investigation, assumptions based on AASHTO (1996) standard specifications for concrete slabs were

considered. AASHTO distinguishes between two types of slabs supported at two edges: reinforced perpendicular to the axis of traffic and reinforced parallel to the axis of traffic. The optimization of the deck has been done without considering the required properties of the deck, such as the performance of the composite and the design between the deck and its supports. Advantages such as increasing the hardness and resistance of the system as well as the economic design of the bridge regarding the performance and layout of the composite should be considered. In this case, the bending behavior of the deck in the plane will be very effective, and this motivation and interest made the performance advantages of the composite core in the bridge deck to be selected for study. An example of the geometry of triangular FRP bridge deck panels is shown in Figure 4.
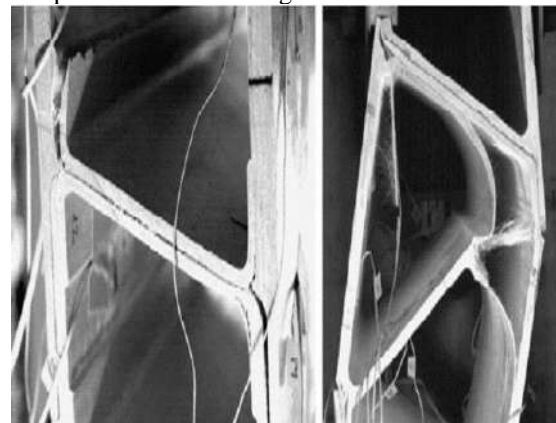

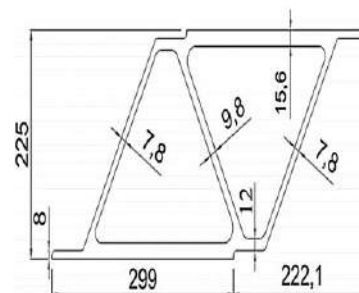Fig. 3. Break in the triangular panel [1]

Fig. 4. An example of a triangular cross section geometry in an FRP deck [1]

The shear failure of FRP sandwich panels is completely different from the shear failure observed

for reinforced concrete structures. According to the published documents, the shear rupture of the panels usually begins with the tearing and separation of the upper surface from the core. Therefore, an FRP panel fails in shear when the shear stress between the top and core interface reaches the contact shear strength. Figure 5.
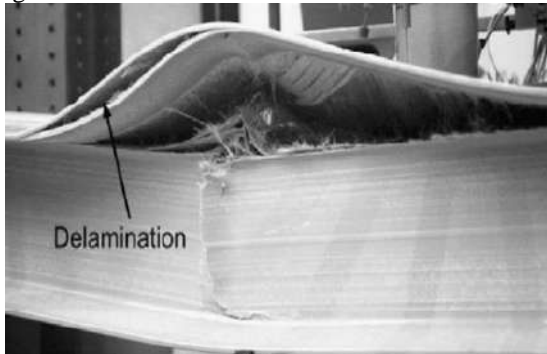

Fig. 5. Shear failure in FRP bridge deck [1]

2. Slab production process

Honeycomb core panels are generally constructed for one-way bending around the x2 axis as shown in. For this reason, most of the past research has focused on the tensile strength of materials around the x1 axis. This study focuses on the load-carrying behavior of glass fiber reinforced polymer (GFRP) bridge deck panels manufactured by Kansas Structural Composites, Inc. (KSCI) using a hand lay-up technique. The deck panels are constructed using a sandwich panel configuration, which consists of two stiff faces separated by a lightweight core. The core has a sinusoidal wave configuration in the x1-x2 plane, as shown in Figure 6.

The sinusoidal wave has an amplitude of 2 in. and the core material has a thickness of 0.09 in., as shown in Figure 6-1(b). Figure 6-1(b) shows a Representative Volume Element (RVE), which is a single basic cell that is repeated periodically to form the core structure. The panel was designed for one-way bending about the x2 axis. Therefore, the bending stiffness about the x2 axis is much higher than that about x1. Plunkett (1997) described in detail the panel manufacturing process. The honeycomb core is composed of a flat GFRP sheet bonded to a corrugated GFRP sheet as shown in Figure

2-1. The core flat parts are laid up on a flat surface with vinylester resin manually applied to chopped strand mat reinforcement. The corrugated parts are fabricated in the same fashion as the flat parts but on corrugated molds. The flat parts are then placed on top of the wet corrugated parts to produce a bond as the corrugated parts cure. The face is composed of fiberglass fabric layers, which are wet in resin and laid up upon each other until desired face thickness is obtained. To increase the interface shear strength between the core and the faces, a new detail is introduced in the manufacturing process for the O'Fallon Park bridge panels. In the panels, GFRP mats are inserted between the core and the faces at about 13 in. distance as shown in Figure 7(b)
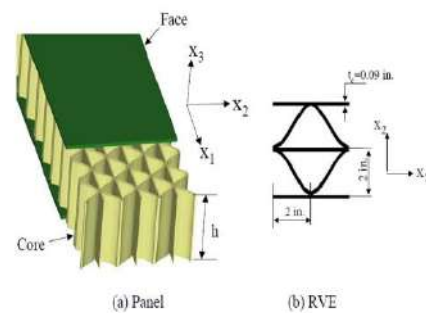

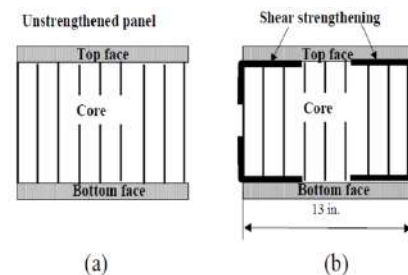Fig. 6. Configuration of the core and the faces [1]

Fig. 7. Shear strengthening details

3. Design Requirements

For this bridge, the design live load specified is an HS 25 truck. This leads to a design wheel load of 20 kips. With an impact factor of 30%, the design load becomes 26 kips per wheel. Tire Contact Area in the AASHTO LFRD Specifications (1998), the tire

contact area is considered a rectangle with a width of 20 in. and a length l given by:

$$l = 2.28\gamma \left(1 + \frac{IM}{100}\right) P \qquad (1)$$

Where γ is the load factor, IM is the impact factor, and P is the wheel load. For this case, $\gamma = 1.75$, IM = 30, and P=20 kips. Hence, l=19 in. which leads to a contact area of 380 square inches.

The load transfer capability of a honeycomb panel is not well understood. Therefore, to determine the effective width for design, some assumptions are necessary. For this evaluation, assumptions were made based on the AASHTO Standard Specifications (1996) for concrete slabs. AASHTO distinguishes

between two cases for slabs supported along two edges: (1) main reinforcement perpendicular to the traffic, and (2) main reinforcement parallel to the traffic. In the first case, the live load moment for a simple span shall be determined by the following formula (impact not included):

$$M = \left(\frac{S + 2}{32}\right) P \ Moment\ on\ foot - pounds\ per\ foot \qquad (2)$$
$$- width\ of\ slab$$

Where S is the effective span length in feet and P is the wheel load in pounds. For slabs continuous over more than two supports, the effective span is defined as the clear span. To estimate the effective bending width for a one-way slab, the load per foot-width of a slab is given as:

$$P = \frac{4M}{S} \ load\ in\ pounds\ per\ foot - width\ of\ slab \qquad (3)$$

The effective bending width in feet is then calculated as follows:

$$W_b = \frac{P}{\bar{P}} \qquad (4)$$

Deflection Criterion According to the City and County of Denver provisions, the panel should be designed so that the deflection due to service load plus impact shall not exceed 1/1000 of the span length. Flexure Criteria Section 600 of the City and County of Denver provisions suggests using both Allowable Stress Design and Load Factor Design approaches as follows. The maximum strain shall be limited to 20% of the ultimate strain under service loads and the maximum dead load strain shall be limited to 10% of the ultimate strain.

The maximum Factored Load shall be given by:

$$P = 1.3x(1.67x(LLxIM) + DL) \qquad (5)$$

and it shall not exceed 50% of ultimate load capacity. In equation (4.5), LL is the Live Load, IM is the Impact Factor, and DL is the Live Load.

Shear Criteria The shear failure mode for the honeycomb sandwich panel used for the O'Fallon bridge deck is expected to be different from that for reinforced concrete (RC) decks. GFRP sandwich deck fails in shear when a face delaminates from the core, and previous experimental studies (Stone et al. 2001 and Lopez 2001) have shown that this mode is most often the governing failure mode for this type of panel. The shear failure mode for the honeycomb sandwich panel used for the O'Fallon bridge deck is expected to be different from that for reinforced concrete (RC) decks. GFRP sandwich deck fails in shear when a face delaminates from the core, and previous experimental studies (Stone et al. 2001 and Lopez 2001) have shown that this mode is most often the governing failure mode for this type of panel. Section 600 of the City and County of Denver provisions indicates that the maximum Factored Load shall be given by equation (4-5) and it shall not exceed 45% of the ultimate shear load capacity of the deck.

Crushing Criteria, the crushing failure load can be calculated by assuming a contact area of 380 in.2 (AASHTO 1998). According to the provisions of the City and County of Denver (2002), the maximum Factored Load shall be given by equation and it shall not exceed 45% of the crushing failure load.

Thermal Expansion Section 600 of the City and County of Denver provisions states that the supplier has to demonstrate through analysis or testing that the FRP bridge deck structure is thermally compatible with both steel and concrete girder systems.

4. Experiment-Based Modeling

The first verification has used Guido Camata experimental model [3], which tested the honeycomb-shaped slab with a sinusoidal cross-section, and we have used the following method:

1- Modeling the modeled sample of TEST2 under cover analysis by changing the location in the middle of the opening with Abaqus software.
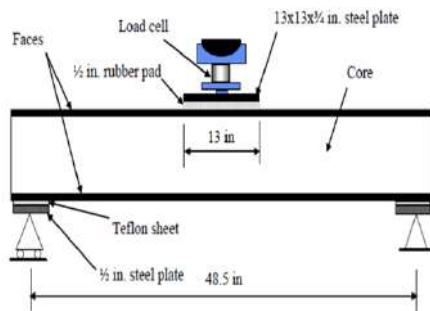
Fig. 8. Geometrical characteristics of the loaded beam [3]

Table. 1.
Geometrical characteristics of the tested beam [3]

	b	h	s	H	H	I
	in	in	in	in	in	in⁴
Test1	13	6.5	0.375	7.25	7.43	155
Test2	12	6.5	0.375	7.25	7.43	143
Test3	13	6.5	0.5	7.5	7.68	201
Test4	13	6.5	0.5	7.5	7.68	201

2- Comparing the outputs obtained from the TEST2 model from the Abaqus software with the results obtained from the laboratory.

In short, we can say that after introducing the materials to the Abaqus software, the modeled sample TEST2 has been subjected to wear analysis by applying displacement in the middle of the opening, the results of which are given in the following discussion. As shown in Figure 8, according to the experiments conducted by Guido Camata who tested the honeycomb slab with sinusoidal cross-section, the geometric characteristics of this beam are given in Table 1.

We used the research of Mr. Davalos [4] to introduce the materials. In this article, micromechanics theories are presented for calculating isotropic materials for modeling composite slabs, both as a real geometric cross-section of the slab and very simplified for manual calculations using an equivalent cross-section. The characteristics of its isotropic materials are presented according to table (2).

Figure 9 shows how force is applied to the beam in the laboratory. Figure 10 shows the separation of the upper part from the core of the beam under load in the laboratory. After the separation of the upper part from the core of the beam under load, it showed its resistance in the form of buckling of the slab

components. What is clear is that the shear reinforcement is for the beam at this time, and it has caused a better cohesion of the slab and prevented its immediate separation and caused it to behave more malleable.

Fig.9 .How to apply force in the laboratory [3]

Fig.10. Separation of the upper surface from the core of the beam under load in the laboratory [3]
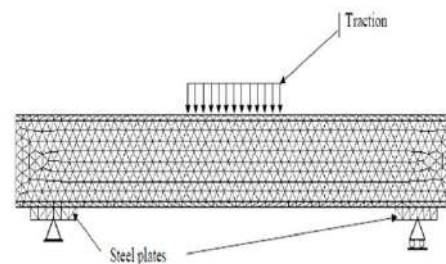

Fig.11. Schematic loading on beam [3]

As mentioned above, shear reinforcement is used to prevent the instantaneous buckling of the slab after the separation of the top from the core, but before the separation, it increases the bending strength due to the increase in the thickness of the top.

Table 2

Layer stiffness properties obtained from micromechanics model

Ply name	Orientation	E_1(Gpa)	E_2(Gpa)	G_{12}(Gpa)	G_{23}(Gpa)	v_{12}	v_{23}
Bond layer	Random	9.72	9.72	3.5	2.12	0.394	0.401
CM3205	0^0or 90^0	27.72	8.00	3.08	2.88		0.390
	Random	11.79	11.79	4.21	2.36	0.295 0.402	0.400
UM1810	0^0	30.06	8.55	3.30	3.08		0.386
	Random	15.93	15.93	5.65	2.96	0.293 0.409	0.388
Core mat	Random	11.79	11.79	4.21	2.97	0.402	0.388

stiffness properties laminates

	E_X,GPa(*10^6 psi)	E_Y,GPa(*10^6 psi)	V_{xy}	G_{xy},GPa(*10^6 psi)
Face laminate	19.62(2.846)	12.76(1.850)	0.302	3.76(0.546)

Figures 11 and 12 show the schematic loading on the beam and its details. This figure indicates that the applied load has occurred in the middle of the beam.
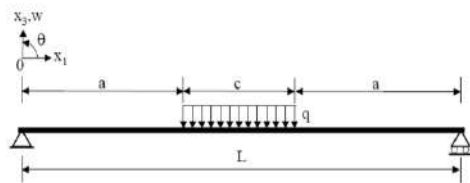

Fig. 12. Schematic loading details on beam

Figure 13 shows the force diagram in terms of displacement of the laboratory sample. This graph indicates that at a force of 80 kips, the displacement will be 0.6.
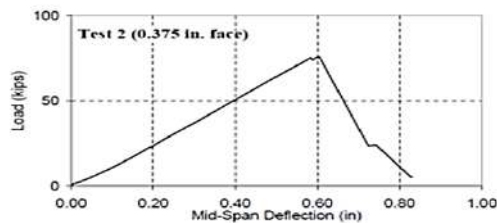

Fig.13. Force diagram according to the change of location of the laboratory sample [3]

5. Modeling with Abaqus finite element software

After introducing the materials to the Abaqus software, the modeled sample TEST2 is subjected to bearing analysis by applying a displacement in the middle of the opening, and during the entire loading period, the resulting force is stored in one of the beam supports, and according to the beam, the applied force in the middle of the opening is equal to twice the reaction value of the support, and in this way, the diagram of the applied force in the middle of the opening according to the displacement according to Figures 16 is drawn, and by comparing it with the laboratory sample, it can be concluded that the behavior of the finite element model is completely similar. According to the laboratory results, it has shown itself. Figure 14 shows the diagram of the force in terms of displacement of the finite element model, which will have a displacement of 0.6 at a load of 70 kips. Figure 15 shows the force diagram in terms of displacement of the laboratory sample, which will have a displacement of 0.6 at a load of 79 kips. Figure 16 is the diagram of the force according to the displacement of the laboratory sample and the software model which shows the comparison of these

two states. These two graphs indicate that the laboratory model has a difference of 1.1%. And the difference is acceptable and the results are very close.
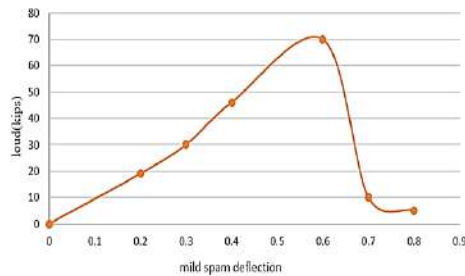

Fig.14. Force diagram according to displacement of the finite element model
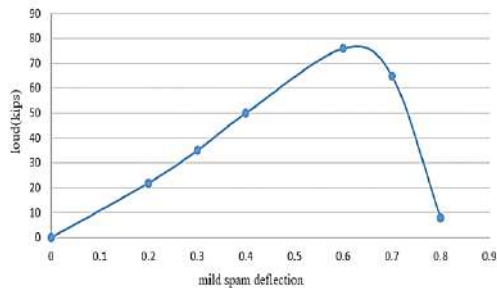

Fig.15. Force diagram according to the change of location of the laboratory sample
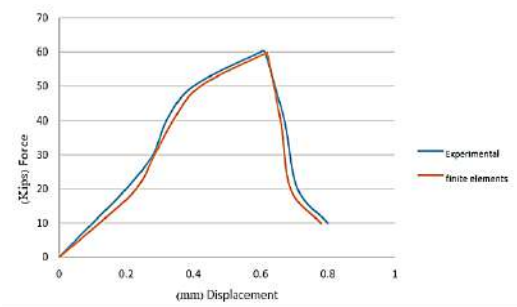

Fig.16. Force diagram according to the change of location of laboratory sample and software model

During loading, after the load reached 70 kips, a slight drop was observed at this point, which indicated the beginning of separation of the top from the core. Finally, the separation spread along the length of the

beam and caused the member to break in a brittle manner.

Figure 17 shows the final deformation of the TEST2 finite element model. This figure indicates that there is a concentration of stress on the middle of the opening, which was subjected to a higher load. Also, the stress in the middle of the thickness of the beam indicates that diagonal cracks will occur in the central areas. In the finite element model, the maximum stress is formed in the middle of the opening, which indicates that the maximum bending stress caused the separation of the upper surface from the core, and since the upper surface is under pressure, a brief buckling in any defect will cause the separation of the core from the surface.
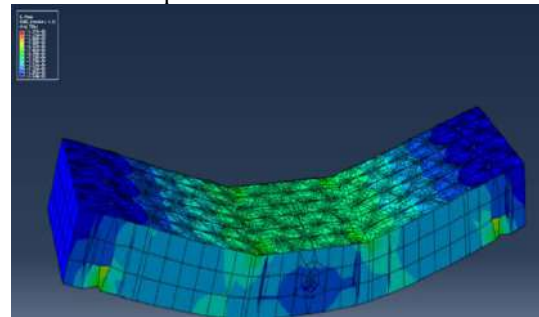

Fig.17. The final transformation of the finite element model TEST2

The abacus model was modified to strengthen against shear, that is, the thickness in the bold parts shown in the figure was 0.09+0.375 inches (Figure 18).
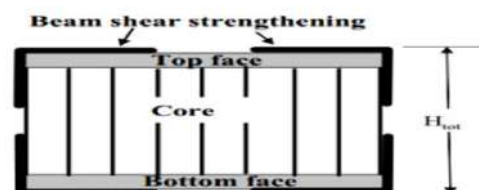

Fig.18. Modified sample

Figure 19 shows the final deformation of the modified TEST2 finite element model. This figure indicates that there is a stress concentration on the pressure area in the middle of the opening, which was subjected to a higher load, and its value will be equal to 1.26 mp. In this part, the ability to create constraints in the area along the support sheet of the software was used. This constraint is introduced to the software in

such a way that the opening length of 48.5 inches is maintained for the finite element model, and also in the area 7.5 inches long from the ends of both sides of the slab, all the element nodes in this area have the same slope according to the reference point that has a vertical support reaction.
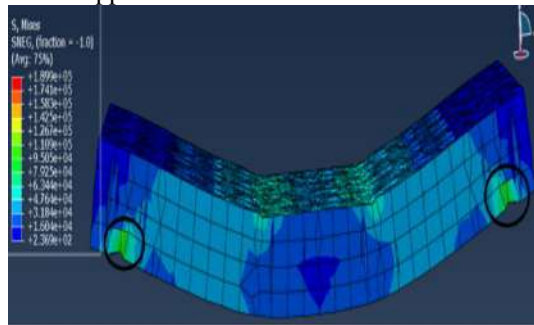

Fig.19. The effect of stress concentration on the local deformation of the modified honeycomb slab at the support

Figure 20 shows the displacement tensor of the beam. This figure indicates that the maximum displacement in the middle of the beam is about 2.2 mm.
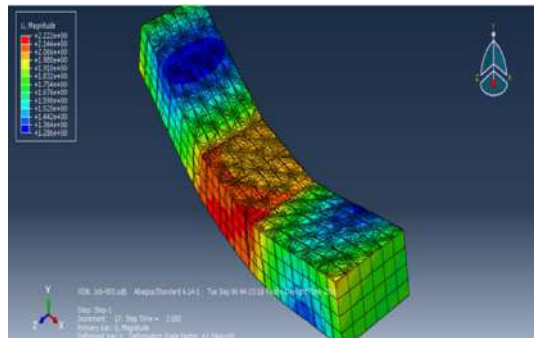

Fig.20. Beam displacement tensor

Figure 21 shows the primary and secondary deformation. And it indicates that the most deformation is related to the middle opening of the beam.

Figure 22 is a diagram showing the shape of the structure. In the case of KIPS70, the maximum displacement is equal to 0.57.

In Figure 23, the shape change diagram of the modeled structure can be seen, which shows the shape change of the structure. In the KIPS70 load, the maximum displacement is equal to 0.5.
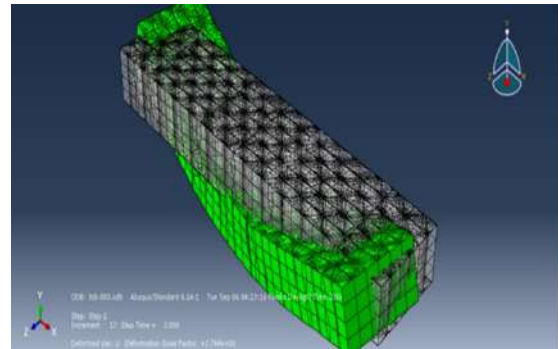

Fig.21. Primary and secondary deformation
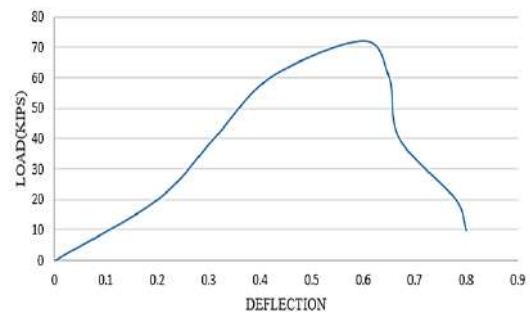
Fig.22. Deformation of the structure in the laboratory
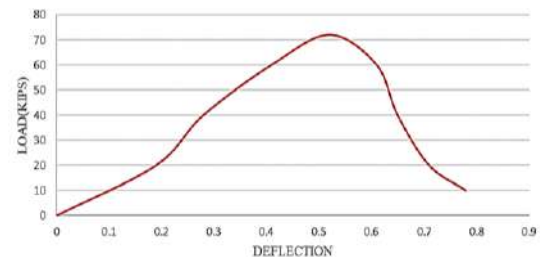

Fig.23. Deformation of the structure in the software in the middle of the opening of the honeycomb slab

Figure 24 shows the comparison diagram of the structural deformation in the software and laboratory model.

Figure 25. The diagram shows stress by distance. This diagram indicates that the maximum stress is on the 25th distance. The intermediate spaces will tolerate the most deformation.
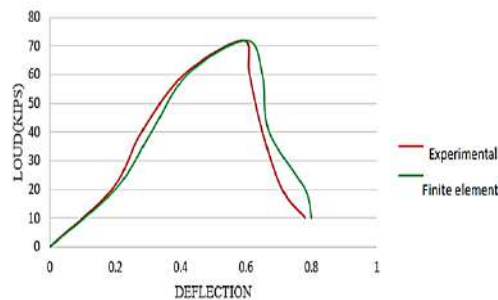
Fig.24. Comparison of structural deformation in the software and laboratory model in the middle of the opening of the honeycomb slab
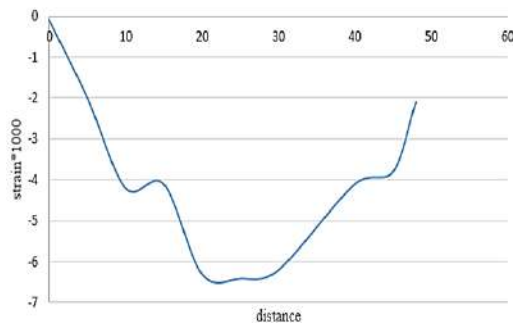

Fig.25. Stress diagram based on distance

6. Conclusion

Comparison of structure deformation in software and laboratory model It indicates that there is not much difference between the obtained results. And the slight difference between the laboratory model and the finite element model is due to the flaws in the laboratory model. According to the initial reports, at the beginning of loading, some of the lamina wires were broken, which had a significant sound. In the finite element model, the maximum stress is formed in the middle of the opening, which indicates that the maximum bending stress caused the separation of the upper surface from the core, and since the upper surface is under pressure, a brief buckling in any defect will cause the separation of the core from the surface. Therefore, this type of member can be investigated and concluded under bending in the finite element model.

Acknowledgments

References

[1] Zihong Liu Thomas E. Cousins, Co-Chair, John J. Lesko, Co-Chair, Raymond H. Plaut, Carin L. Roberts Wollmann and Elisa Sotelino. (2007). "Testing and Analysis of a Fiber-Reinforced Polymer (FRP) Bridge Deck", Doctor of Philosophy in Civil Engineering, Virginia Polytechnic Institute and State University.

[2] Aixi Zhou, John J. Lesko, Co-Chairman, Thomas E. Cousins, Co-chairman, Romesh C. Batra, Scott W. Case and Liviu Librescu. (2002), "STIFFNESS AND STRENGTH OF FIBER REINFORCED POLYMER COMPOSITE BRIDGE DECK SYSTEMS", Doctor of Philosophy in Engineering Mechanics", Blacksburg, Virginia, USA

[3] Guido Camata, P. Benson Shing. (2004) "EVALUATION OF GFRP DECK PANEL FOR THE O'FALLON PARK BRIDGE" COLORADO DEPARTMENT OF TRANSPORTATION RESEARCH BRANCH July 2004.

[4] Davalos, J. F., Qiao, P., Xu, F. X., Robinson, J., and Barth, K. E. 2001."Modeling and characterization of fiber-reinforced plastic honeycomb sandwich panels for highway bridge applications." Compos. Struct., 523–4, 441–452.

[5] American Association of State Highway and Transportation Officials (AASHTO), "Specifications for Highway Bridges", Washington, 17th Edition, 2010.

[6] Japan Road Association., (1998)., "Reference For Seismic Retrofit of Existing Highway Bridges", Maruzeh, Tokyo., Japan.vol. 195. pp.35-45.

Author Guidelines EditEdit Author Guidelines

GENERAL GUIDELINES FOR AUTHORS

Journal of civil engineering researches invites unsolicited contributions of several forms: articles, reviews and discussion articles, translations, and fora. Contributions should fall within the broad scope of the journal, as outlined in the statement of scope and focus. Contributors should present their material in a form that is accessible to a general anthropological readership. We especially invite contributions that engage with debates from previously published articles in the journal.

Submissions are double-blind peer-reviewed in accordance with our policy. Submissions will be immediately acknowledged but due to the review process, acceptance may take up to three months. Submissions should be submitted via our website submission form (see links above for registration and login). Once you login, make sure your user profile has "author" selected, then click "new submission" and follow the instructions carefully to submit your article. If problems arise, first check the FAQ and Troubleshooting guide posted below. If you are still experiencing difficulty, articles can be submitted to the editors as email attachments.

Each article should be accompanied by a title page that includes: all authors' names, institutional affiliations, address, telephone numbers and e-mail address. Papers should be no longer than 10,000 words (inclusive of abstract 100-150 words, footnotes, bibliography and notes on contributors), unless permission for a longer submission has been granted in advance by the Editors. Each article must include a 100 words "note on contributor(s)" together will full institutional address details, including email address. We request that you submit this material (title page and notes on the contributors) as "supplementary files" rather than in the article itself, which will need to be blinded for peer-review.

We are unable to pay for permissions to publish pieces whose copyright is not held by the author. Authors should secure rights before submitting translations, illustrations or long quotes. The views expressed in all articles are those of the authors and not necessarily those of the journal or its editors. After acceptance, authors and Special Issue guest editors whose institutions have an Open Access library fund must commit to apply to assist in article production costs. Proof of application will be requested. Though publication is not usually contingent on the availability of funding, the Journal is generally under no obligation to publish a work if funding which can be destined to support open access is not made available.

Word template and guidelines

Our tailored Word template and guidelines will help you format and structure your article, with useful general advice and Word tips.

(La)TeX template and guidelines

We welcome submissions of (La)TeX files. If you have used any .bib files when creating your article, please include these with your submission so that we can generate the reference list and citations in the journal-specific style

Artwork guidelines

Illustrations, pictures and graphs, should be supplied with the highest quality and in an electronic format that helps us to publish your article in the best way possible. Please follow the guidelines below to enable us to prepare your artwork for the printed issue as well as the online version.

Format: TIFF, JPEG: Common format for pictures (containing no text or graphs).

EPS: Preferred format for graphs and line art (retains quality when enlarging/zooming in).

Placement: Figures/charts and tables created in MS Word should be included in the main text rather than at the end of the document.

Figures and other files created outside Word (i.e. Excel, PowerPoint, JPG, TIFF, EPS, and PDF) should be submitted separately. Please add a placeholder note in the running text (i.e. "[insert Figure 1.]")

Resolution: Rasterized based files (i.e. with .tiff or .jpeg extension) require a resolution of at least 300 dpi (dots per inch). Line art should be supplied with a minimum resolution of 800 dpi.

Colour: Please note that images supplied in colour will be published in colour online and black and white in print (unless otherwise arranged). Therefore, it is important that you supply images that are comprehensible in black and white as well (i.e. by using colour with a distinctive pattern or dotted lines). The captions should reflect this by not using words indicating colour.

Dimension: Check that the artworks supplied match or exceed the dimensions of the journal. Images cannot be scaled up after origination

Fonts: The lettering used in the artwork should not vary too much in size and type (usually sans serif font as a default).

Authors services:

For reformatting your manuscript to fit the requirement of the Journal of Civil Engineering Researchers and/or English language editing please send an email to the following address:

researchers.services@gmail.com

Noted: There is a fixed charge for these mentioned services that is a function of the manuscript length. The amount of this charge will be notified through a reply email.

FAQ AND TROUBLESHOOTING FOR AUTHORS

I cannot log in to the system. How do I acquire a new user name and password?

If you cannot remember your username, please write an email to (journals.researchers@gmail.com), who will locate your username and notify you. If you know your username, but cannot remember your password, please click the "Login" link on the left-hand menu at homepage. Below the fields for entering your username and password, you will notice a link that asks "Forgot your password?"; click that link and then enter your email adddress to reset your password. You will be sent an automated message with a temporary password and instructions for how to create a new password. TIP: If you do not receive the automated email in your inbox, please check your SPAM or Junk Mail folder. For any other issues, please contact our Managing Editor,Kamyar Bagherinejad (admin@journals-researchers.com).

How do I locate the online submission form and fill it out?

First you need to register or login (see above). Once you are logged in, make sure the "roles" section of your profile has "Author" selected. Once you assign yourself the role of "Author," save your profile and then click the "New Submission" link on your user home page.

Once you arrive at the submission form page, please read the instructions carefully filling out all necessary information. Unless specified otherwise by the editors, the journal section to be selected for your submission should be "Artlcles." Proceed to the remaining sections, checking all boxes of the submission preparation checklist, and checking the box in the copyright notice section (thus agreeing to journals-researchers's copyright terms). Once the first page is completed, click "Save and Continue." The next page allows you to upload your submission. Use the form to choose your file from your computer. Make sure you click "Upload." The page will refresh and you may then click "Save and Continue." You will then proceed to a page for entering the metadata for your article. Please fill out all required fields and any further information you can provide. Click "Save and Continue." The next page allows you to upload supplementary files (images, audiovisual materials, etc.). These are not required, but if you wish to provide supplementary materials, please upload them here (do no forget to click "Upload." Then click "Save and Continue." This brings you to the final page of the submission form. Please click "Finish Submission" in order to close the

submission process. You wil then be notified by email that your article has been successfully submitted. TIP: If you do not receive the automated email in your inbox, please check your SPAM or Junk Mail folder. For any other issues, please contact our Managing Editor, Kamyar Bagherinejad (admin@journals-researchers.com).

Why am I not receiving any email notifications from HAU?

Unfortunately, some automated messages from Open Journal Systems arrive in users' Spam (or Junk Mail) folders. First, check those folders to see if the message was filtered into there. You may also change the settings of your email by editing your preferences to accept all mail from [jcer] and related journals-researchers.com email accounts.

I am trying to upload a revised article following an initial round of peer-review, but I cannot locate where to upload the article. Where do I submit a revised article?

Follow the login process outlined above and when you successfully login you will see on your user home page a link next to "Author" for "active" articles in our system (usually it is only one article, but if you have mulitple submissions currently in our system, the number could be higher. Click the "Active" link and you will be led to a page that lists your authored articles currently in our system. Click the link under the column labeled "Status" and this will take you to a page showing the current review status of your article. At the very bottom of the screen, you will see an upload form under the heading "Editor decision." Here you may upload your revised article. An automated email will be sent to the editors and you may also notify them directly via email. You may then logout.

I successfully submitted an article; how long will it take for the editors to respond to me with a decision.

For all articles that are recommended for peer-review, the editors of JCER strive to notify authors of a decision within 4-6 weeks. You may contact JCER's Managing Editor, Kamyar Bagherinejad (admin@journals-researchers.com). if you have any questions relating to the review process and its duration.

For all other inquiries, please contact: Kamyar Bagherinejad (Managing Editor)

Privacy Statement

The names and email addresses entered in this journal site will be used exclusively for the stated purposes of this journal and will not be made available for any other purpose or to any other party.

Articles

Section default policy

Make a new submission to the Articles section.

Copyright Notice EditEdit Copyright Notice

Journal of Civil Engineering Researchers follows the regulations of the International Committee on Publication Ethics (COPE) and the ethical principles of publishing articles in this journal are set based on the rules of this committee, and in case of problems, it will be treated according to these rules.

This work is licensed under a Creative Commons Attribution 4.0 International License (CC BY 4.0).

In short, copyright for articles published in this journal is retained by the authors, with first publication rights granted to the journal. By virtue of their appearance in this open access journal, articles are free to use, with proper attribution and link to the licensing, in educational, commercial, and non-commercial settings

Privacy Statement EditEdit Privacy Statement

The names and email addresses entered in this journal site will be used exclusively for the stated purposes of this journal and will not be made available for any other purpose or to any other party.

Scholars Pavilion

Scholars Pavilion or **Scholars Chartagi** is a monument donated by the Islamic Republic of Iran to the United Nations Office at Vienna. The monument architecture is claimed by the Islamic Republic News Agency of Iran to be a combination of Islamic and Achaemenid architecture, although the latter clearly predominates in the decorative features, with Persian columns and other features from Persepolis and other remains from the Achaemenid dynasty. The Chahartaq pavilion form runs through the architecture of Persia from pre-Islamic times to the present.

Statues of four famous Persian medieval scholars, Omar Khayyam, Al-Biruni, Muhammad ibn Zakariya al-Razi and Ibn-Sina are inside the pavilion. This monument donated in June 2009 in occasion of Iran's peaceful developments in science.

J-Researchers